Title: An efficient domain decomposition framework for accurate representation of geodata in distributed hydrologic models

Authors:

1) Mukesh Kumar
Research Assistant
212 Sackett Bldg.
Dept. of Civil and Environmental Engineering
Penn State University, University Park, 16802
muk139@psu.edu

2) Gopal Bhatt
Research Assistant
212 Sackett Bldg.
Dept. of Civil and Environmental Engineering
Penn State University, University Park, 16802
gxb913@psu.edu

3) Christopher J. Duffy (Corresponding Author)
Professor
212 Sackett Bldg.
Dept. of Civil and Environmental Engineering
Penn State University, University Park, 16802
cxd11@psu.edu

Keywords: Domain Decomposition; Mesh Generation; Constrained Delaunay Triangulation; Hydrologic Modeling; Geodata Representation

Abstract

Physically-based, fully-distributed hydrologic models simulate hydrologic state variables in space and time while using information regarding heterogeneity in climate, land use, topography and hydrogeology. Since fine spatio-temporal resolution and increased process dimension will have large data requirements, there is a practical need to strike a balance between descriptive detail and computational load for a particular model application. In this paper we present a flexible domain decomposition strategy for efficient and accurate integration of the physiographic, climatic and hydrographic watershed features. The approach takes advantage of different GIS feature types while generating high-quality unstructured grids with user-specified geometrical and physical constraints. The framework is able to anchor the efficient capture of spatially distributed and temporally varying hydrologic interactions and also ingest the physical prototypes effectively and accurately from a geodatabase. The proposed decomposition framework is a critical step in implementing high quality, multiscale, multiresolution, temporally adaptive and nested grids with least computational burden. We also discuss the algorithms for generating the framework using existing GIS feature objects. The framework is successfully being used in a finite volume based integrated hydrologic model. The framework is generic and can be used in other finite element/volume based hydrologic models.

1. Introduction

Distributed models simulate hydrologic states in space and time while using discretized information regarding the distribution and parameters of climate, land use, topography and hydrogeology (Feeze and Harlan 1969). These models have inherent advantages over conventional lumped models particularly because natural heterogeneities control watershed behavior(s) and also help in resolving the feedback processes between state variables (Entekhabi and Eagleson 1989; Pitman *et. al.* 1990). The numerical solution strategies require spatial discretization of the model domain into spatially connected units. For example grid decomposition for land surface models may take advantage of relevant physical subdomains such as hillslopes (Band 1986), a contour (Moore *et. al.* 1988), structured (Panday and Huyakorn 2004) or unstructured grids (Qu and Duffy 2007). In the case of multi-process/multi-scale models, the representation of topography, land cover, soil, geology, vegetation and climate on a distributed model grid must, by necessity, deal with questions of computational efficiency and limits of parameterization. Since our goal is to perform physics based simulations on large watersheds, our strategy is to minimize the resolution of spatial discretization (fewest number of elements to preserve the essential physics) while still capturing the local heterogeneities in parameters and process dynamics. We achieve this by generating conformed Delaunay triangulation by using distributed GIS anchor objects like points, lines and polygons.

2. Domain decomposition: Limitations and scope

Geometrically, the quality (shape and size) and type of the discrete elements which make up the model grid determines the accuracy, convergence, memory storage and computational cost of the numerical solution. Physically the decomposed domain must admit a) conformity with the boundary b) connectivity between elements and c) continuity of mass within each terrain element. The use of rectangular grids with uniform topological structure have seen wide use for domain discretization for integrated hydrologic models such as PARFLOW-Surface Flow (Kollet and Maxwell 2006) and MODHMS (Panday and Huyakorn 2004). The inherent simplicity of a structured grid has the advantage of fast computations for linear/nonlinear systems because of uniformity in the size of neighboring grids and the ease of determining grid's neighbors. Furthermore, the regularity of structured meshes makes it straightforward to parallelize computations. More to the point, it also complements the data ingestion process for spatially distributed geologic, topographic and meteorologic data that are available as raster maps/images. The computational advantage of modeling on structured grids is sometimes offset by the need for very fine spatial discretization in order to capture local heterogeneities and boundary "edges". Rigidness of the regular grids prevents the resolution of relatively small topological structures without either resorting to a higher spatial resolution or using a nested or adaptive mesh refinement (Blayo and Debreu, 1999). Structured meshes also lack flexibility in fitting complex-shaped domains. Techniques have been devised to find appropriate coordinate transformations like conformal mapping and algebraic methods which would lead to better fitting of irregular shapes (Castillo 1991, Thompson 1982). However these methods are complex and introduce errors due to interpolation of derivatives. The "Staircase effect" at the boundaries is observed when no transformation is applied. No matter how fine the resolution of the regular grid is, linear features which are not aligned in the principal direction of the grid are "aliased". This redefinition of boundaries because of gridding at different spatial scales, particularly at places where hydrologic properties undergo a transition like a land cover change from forest to urban or a topographic changeover, significantly affects the modeling of movement of matter and energy (Woo 2004). Structured mesh representations also restricts surface flow directions to 45-degree increments (Tarboton 1997) which can introduce anisotropy in preferred flow direction (Braun and Sambridge 1997). Finally, regular grids create complications for Nuemann-type boundary conditions as they are forced to align in the two principal orthogonal directions along which the grid is oriented. Figure 1 provides an example of the aliased boundary representation for the Little Juniata watershed in central Pennsylvania.

Many of these limitations can be overcome by using a decomposition strategy based on Triangular Irregular Networks (TINs) (Goodrich 1990, Jones *et. al.* 1990, Vivoni *et. al.* 2004, Ivanov *et. al.* 2004) or generalized unstructured meshes (Qu and Duffy 2007). The advantage of an unstructured mesh is that it can provide an "optimal" representation of the domain with the least number of elements while still conforming to limited set of physical and geometric constraints. The unstructured grid leads to a large decrease in the number of nodes/elements with respect to structured meshes (Shewchuk 1996). Also, it allows better representation of line-features such as the stream network, land-use/ land-cover boundaries and watershed boundaries. In order to unlock the full potential of unstructured mesh decomposition, we generate them in a "smart" way by using GIS feature objects. This approach leads to discrete domains that are

computationally efficient and which honor the edges and transitions of the important physiographic, geologic, ecologic and hydroclimatic variables. The next section discusses unstructured grid representations for integrated hydrologic modeling.

3. Solving multiple processes on an unstructured mesh

There are two approaches to solving systems of hydrologic equations simultaneously. The first is a weakly coupled approach where water and energy exchange between surface water, groundwater, vegetation and atmosphere are solved separately on different discretized domains while sharing interaction flux as individual boundary conditions. The physical interaction in this case is weakly coupled in that the communication between processes is intermittent and only occurs as necessary to satisfy conservation or efficiency constraints. The synchronization of communication is performed by controller software. Since the decomposition framework for each individual physical process is separate, data assignment, topology definitions, data geo-registration and flux exchange between different physical components of the models is an error prone and computationally intensive approach. Weakly coupled models are also susceptible to convergence problems (Abbot et. al. 1986) and unreliable solutions (Fairbanks et. al. 2001). The second strategy can be referred as "full" volume coupling, where all the physical process equations are solved simultaneously on each element distributed across the domain. For the purposes of this paper, there are important advantages to the volume-coupling approach in that the approach offers a consistent and uniform assignment and registration of geo-data for all the physical model equations and for all discrete elements in the domain. The Penn State Integrated Hydrologic Model (PIHM, Kumar et. al. 2008, Qu and Duffy 2007) uses the latter approach and is briefly described next.

PIHM is a semi-discrete finite volume method (FVM) based numerical model. It solves ordinary differential equations (ODE) corresponding to all the interacting hydrologic processes on each discretized watershed element. PIHM uses implicit Newton-Krylov integrator available in the CVODE (Cohen and Hindmarsh 1994) to solve for state variables at each time step. The discretized control volume elements used in PIHM are either triangular or linear in shape as shown in Figure 2. Triangular land surface elements are projected downwards to the bedrock or regolith to form a prismatic element in 3D. Linear elements represent rivers and are projected downwards to the river bed. The model is designed to capture “dynamics” in multiple processes while maintaining the conservation of mass at all cells, as guaranteed by the finite volume formulation. The finite volume formulation also has the ability to handle discontinuous solutions (Leveque 2002). The conservation laws that are conveniently derived from the physical relationships approximate the average state of the process variable over the kernel volume.

In order to perform accurate and efficient simulations, domain decomposition quality should be considered as important as the numerical scheme itself. Mesh size, shape and the ability to capture graded and/or sharp spatial changes depending on the time scale of the interacting hydrologic processes, spatial gradient of the state variables and the heterogeneity in model parameter distribution determine the stability, convergence and accuracy of the solution. PIHM uses a smart unstructured mesh decomposition that is generated using GIS feature objects to enhance topographic and hydrographic representations, which are discussed in the next section.

4. Unstructured mesh generation and GIS objects

Although theoretical and computational aspects of unstructured meshes have been widely documented in computational fluid dynamics literature (Weatherill 1998), limited efforts have been made to generate them using GIS feature-objects for hydrologic modeling applications. This is in part due to the limited use of unstructured meshes in hydrologic modeling, which have been restricted to TINs only (Ivanov *et. al.* 2004), and also because of the disconnect between data structures of the GIS feature objects and geometric objects used in computational geometry applications. Most of the unstructured meshing tools (e.g. Henry and Walters 1993 and Shewchuk 1997) use points or planar straight line graphs (PSLGs) to generate Delaunay triangulations. This necessitates representation of existing GIS feature objects such as points, lines, polygons, junctions and edges as either points or PSLGs only. A PSLG is a set of vertices and segments that satisfies two constraints – a) PSLG must have two vertices that serve as endpoints b) segments in a PSLG are permitted to intersect only at their endpoints. By reprocessing we can essentially reduce all the different feature objects to either a node or a line, making them suitable for use in traditional unstructured meshing tools.

4.1. Reprocessing of GIS objects

Data structure of points and junctions can have a representation similar to nodes when both are defined with an identifier; a coordinate location and a corresponding attribute. Edges and Polyline features in GIS have data structures similar to PSLGs when defined by an identifier, number of segments in each compound object, and a start and end node identifier for each segment. Edge features also carry additional topology information. A polygon feature can be viewed as a collection of chained polylines that form a closed boundary around individual areas having no gaps or overlaps (Nyerges 1993). Figure 3 shows the data structure of each object type. A GIS representation of a natural watershed is a complex multi-polygon feature composed of subshed boundaries (shown in Figure 2), lakes, wetlands and river reaches. For application to unstructured meshing tools for watershed modeling, multi-polygon features need to be further broken down into simplified polyline features. This is accomplished by disintegrating each polygon feature into polylines at junction (intersection) points or at the entry node of a polygon. The process involves a sequence of four steps- a) Identify polygons that share edges b) Identify the junction nodes of sharing polygons c) Store polyline segments between the two junction nodes or between a junction and an end/start node d) Discard duplicate polyline obtained from either one of the sharing polygons. Identifying the total number of polygons as totPolygon, the pseudocode for transforming multi-polygon into polylines is shown below:

```
PolygonToPolyline():

For i = 0 to totPolygon {
        For j = 0 to (i-1)th Polygon {
                If ((MBD of ith Polygon) ∩ (MBD of jth Polygon)) ≠ NULL {
```

IdentifyJunctionPoints()
Disintegrate() Polygon to PolyLines at junction point(s) and at id = 0
Delete() shared polyline from **j**th Polygon
}
}
}

Appendix:

If ((MBD of **i**th Polygon) $\cap$ (MBD of **j**th Polygon)) $\neq$ NULL
➔ Intersection Area $\neq 0$
➔ Polygon **i** shares junction(s) with Polygon **j**

IdentifyJunctionPoints():

For k = **0** to **numPts_1** in IntersectionArea of Polygon 1 {
For m = 0 to **numPts_2** in IntersectionArea of Polygon 2 {
If (k^{th} Pt1 = m^{th} Pt2) { /* These points are shared by two intersecting/partially overlapping polygons */
/* Following conditions identify a junction node from the shared nodes */
If ((($(k-1)^{th}$ Pt1 = $(m-1)^{th}$ Pt2) ***AND*** ($(k+1)^{th}$ Pt1 $\neq$ $(m+1)^{th}$ Pt2)) ***OR***
($(k-1)^{th}$ Pt1 = $(m+1)^{th}$ Pt2) ***AND*** ($(k+1)^{th}$ Pt1 $\neq$ $(m-1)^{th}$ Pt2)) ***OR***
($(k+1)^{th}$ Pt1 = $(m+1)^{th}$ Pt2) ***AND*** ($(k-1)^{th}$ Pt1 $\neq$ $(m-1)^{th}$ Pt2)) ***OR***
($(k+1)^{th}$ Pt1 = $(m-1)^{th}$ Pt2) ***AND*** ($(k-1)^{th}$ Pt1 $\neq$ $(m+1)^{th}$ Pt2))) {
k^{th} Pt1 and m^{th} Pt2 are Junction Points
}
}
}

Legends:

numPts_*:	Number of points of Polygon * in the Intersection Area
Pt*:	Nodal points belonging to polygon *
MBD:	Minimum Bounding Rectangle

A schematic application of the algorithm on a representative multi-polygon feature is shown in a series of steps in Figure 4. The algorithm has been incorporated in the implementation of PIHMgis (www.pihm.psu.edu/pihmgis/).

With all GIS feature objects being reduced to a point or a PSLG, a domain decomposition tool like TRIANGLE (Shewchuk 1997) can be used for unstructured mesh

decomposition. However the raw polylines and the ones obtained from reprocessing of GIS polygons generally have segment lengths that are very small compared to the dynamical scales of interest in the hydrologic model. The smaller segment lengths are an artifact of DEM-processing based watershed delineation algorithms that are available in ArcHydro (Maidment 2002) and TauDEM tool (Tarboton and Ames 2001). Segments obtained from DEM processing have their lengths determined by the resolution of the DEM used for watershed delineation. Digitized watershed polygon boundaries may be composed of segments with smaller lengths than are needed to efficiently represent process dynamics. Smaller segment lengths translate to generation of unnecessarily small triangles in the vicinity of polylines (as shown in Figure 5) thus also resulting in an excessive number of mesh elements in the model domain. This places an impractical time-step restriction on the model to maintain numerical accuracy and stability (e.g. the Courant–Friedrichs–Lewy (CFL) condition in explicit time-stepping methods, Courant et al. 1928). In order to produce high-quality meshes while still maintaining the fidelity of the internal and external polyline boundaries, reconditioning of polyline needs to be performed.

4.2. Polyline reconditioning

Reconditioning of polyline translates to a simplification of the line boundary by removing small fluctuations or extraneous bends while preserving the essential shape. The approximation error here is controlled by setting a maximum-distance-from-vertex to the approximated polyline criteria. Simplification of polyline is performed based on the Douglas and Peucker (DP) algorithm (1973). The first approximation of the polyline is a line segment connecting the first and last vertices of the polyline. Recursively, the maximum normal departure of each segment of the approximation to the vertices in the original polyline segment is calculated. If the distance from the farthest vertex to this approximate segment is larger than some specified tolerance, then the vertex is added to the approximating polyline. The algorithm terminates when all vertices in the original polyline are within a specified tolerance for distance. Sequential execution of the algorithm on a representative polyline is shown in Figure 6. Pseudocode of the algorithm is shown below:

```
SimplifyLine():

Read points in polyline from 0 to n: Pts[node_0, node_1,……..node_n]
/* Recursive simplification. Starts with selection of end points of a polyline */
Simplify (Pts [], tolerance, 0, n)
Connect all MARKEDnode  to get Simplified Line

.....

Simplify (Pts [], tolerance, i, j) :

/* Find the vertex in original polyline that is farthest from approximate segment */
If (j+1 > k) {
        MAXdistance =0
```

```
        For index = i+1 to j-1 {
                Find distance() of node_index from line segment (node_i ↔ node_j)
                        If (distance() > MAXdistance) {
                                MAXdistance = distance()
                                MARKnode = index
                        }
        }
/* Use the MARKEDnode (that is farthest from approximate segment) to anchor another
set of approximation */
        If (MAXdistance > tolerance) {
                MARKEDnode = MARKnode
                Simplify(Pts[], tolerance, i, index)
                Simplify(Pts[], tolerance, index, j)
        }
}

/* Distance calculation between node_index and segment(node_i ↔ node_j) */
/* node_index = (x3, y3);      node_i = (x1, y1);      node_j = (x2,y2)          */

distance():
```

$$m = \frac{(x3 - x1) * (x2 - x1) + (y3 - y1 * (y2 - y1)}{\|node\_i - node\_j\|^2}$$

$$\text{Distance} = \sqrt{(x3 - (x1 + m(x2 - x1))^2 + (y3 - (y1 + m(y2 - y1))^2}$$

Figure 5 shows how polyline reconditioning results in a reduction in the number of triangles formed particularly near the boundaries. The algorithm has been incorporated in the implementation of PIHMgis (www.pihm.psu.edu/pihmgis/).

4.3. Delaunay Triangulation based mesh generation

By using Very Important Points (VIPs), junctions, observation station nodes, and the boundary PSLGs as constraints, unstructured meshes that satisfy an "empty circle" condition are generated. Such unstructured meshes are called Delaunay triangles. We note that an "empty circle" condition means that the circumcircles of the triangles does not enclose the vertices of any other triangles in the mesh. Delaunay triangulation also satisfies "max-min angle optimality" condition (Lawson 1977). This optimality criteria essentially ensures a high quality triangulation i.e. triangles created have a circumradius-to-shortest edge ratio (say *M*) as small as possible (Miller *et. al.* 1995). This means that the generated triangles are balanced and not skewed. VIPs that are used as constraints during triangulation are obtained by the implementation of VIP algorithm of Chen and Guevara (1987) or Fowler and Little (1979) on a DEM. External boundary polyline which can be either concave or convex, acts as a spatial limit-constraint in decomposition, beyond which no triangles are generated. The tolerance criteria in polyline reconditioning and VIP algorithms determine the degree of approximation of

vector boundaries and raster DEM respectively. Smaller tolerance criteria results in tighter approximations but it also increases the number of unstructured meshes. Figure 7 shows the generation of higher resolution meshes with a decrease in polyline tolerance criteria and increase in number of VIP nodes. For all unstructured mesh decomposition resolutions, triangulations outperform their structured mesh counterparts with the same average resolution in terms of both efficiency and accuracy. Figure 8(a) shows the average root-mean-square error (RMSE) in representation of DEM and its slope by a structured grid decomposition of the watershed relative to an unstructured mesh. RMSE is calculated by evaluating the difference in elevation/slopes for both structured and unstructured grids w.r.t original high resolution DEM. Three decomposition levels for unstructured meshes used in calculation of the error statistics correspond to the decompositions shown in Figure 7. The average structured grid resolution (R_{sg}) is calculated by

$$R_{sg} = \sqrt{\frac{A}{N_{umn}}} \qquad (1)$$

where A is the area of the watershed and N_{umn} is the number of nodes in the unstructured mesh. By this simple measure, unstructured meshes outperform structured meshes at all resolutions and for all criteria considered. Figure 8(b) shows the average "vector error" per unit length of original polyline boundary in capturing its tortuousities by structured and unstructured grids respectively. Vector Error is calculated by calculating the area of the enclosed polygon bounded by original polyline and the corresponding boundary polyline representation used in structure or unstructured meshes. Again unstructured meshes show better performance for the representation of boundary heterogeneities. Obviously with increasing resolution of either type of grids, there is a reduction in the error magnitude. We note that a standard Delaunay triangulation is not sufficiently suited for hydrologic modeling as it does not ensures generation of "quality" triangles and also does not respect the internal boundary constraints.

5. Model and Data Constraints on Decomposition

Depending on the numerical formulation of the physical equations, local topographic gradients and physiographic heterogeneity, generation of unstructured meshes can be customized to enhance representational accuracy and to capture different time scales of process interaction. Customization criteria are generally based on constraints posed by hydrologic model design and data heterogeneity.

5.1. Model constraints

Many of the unstructured mesh based models like PIHM (Kumar *et. al.* 2008, Qu and Duffy 2007) and RSM (Lal *et. al.* 2003) assume that the flux across the triangle edges is always orthogonal. This assumption simplifies the numerical formulation of process equations and also saves extra computation in defining the directional components of the fluxes. The "orthogonal" condition is ensured by considering a circum-center (instead of centroid) as the representative location of triangular elements. We note that the line joining the circumcenter of neighboring triangles will always be perpendicular to the

common side shared by the triangles. Triangulations generated based on a circumcenter formulation also aids diagonal dominance (Baker *et. al.* 1988) and faster convergence of the numerical method (Vavasis 1993). However, as shown in Figure 9, the circum-center of obtuse angled triangles can sometimes fall outside the triangle. To avoid this condition requires a constraint on the triangle shape that all the angles have to be acute. It is evident from Figure 10 that the upper bound on the ratio *M* (circumcenter-to-shortest triangle edge) ensures that the lower bound on the smallest angle of the triangle is $Sin^{-1}(\frac{1}{2M})$ and vice versa (Shewchuck 1996). The lower bound on the smallest angle in turn bounds the largest angle of the triangle also i.e. if the smallest angle is θ then the largest angle can not be larger than 180-2θ. This implies that by manipulating the value of *M*, we can have delaunay triangles with its largest angle bounded. Ruppert's Delaunay refinement algorithm (Ruppert 1995) employs a bound of $M = \sqrt{2}$ which means the angles of the triangles range between 20.7^o and 138.6^o while Chew's Delaunay refinement algorithm (Chew 1993) employs a bound of $M = 1$ which means the angles range between 30^o and 120^o.

Another model constraint desirable for unstructured mesh generation is size. Maximum allowable size of the triangles determines the total number of discretized elements and hence the computational load and memory storage requirements for a simulation. Furthermore, meshes are expected to have the ability to grade from small to large elements over a relatively short distance. A larger value of *M* translates to sharp gradation in triangle size. A Delaunay triangulation algorithm proposed by Bern *et. al.* (1994), Baker *et. al.* (1988) and Hitschfeld and Rivara (2002) generates non-obtuse triangles only, perfect for use in circumcenter based model formulations. Nonetheless, these algorithms have limited flexibility in terms of controlling the upper bound on the number of nodes in triangulation, the implementation of VIPs and PSLGs as internal boundaries and also in terms of spatial gradation in triangle size. The user must settle for a tradeoff between the number of elements in the watershed and the number of triangles that violate the non-obtuse criterion. Ruppert's algorithm (Ruppert 1995) generates nicely graded and optimal-size triangles while relaxing the non-obtuse triangle criteria. This algorithm produces a mesh whose size (number of elements) is at most a constant factor larger than the size of the smallest possible mesh that meets the same angle bound (Shewchuk 1997). For the relatively small percentage of triangles that violate the non-obtuse criterion, the centroid is assumed to be the representative of triangular element.

5.2. Data constraints

Thematic spatial data that relate hydrographic and hydrogeologic parameters (e.g. soil maps, stream cross-sections and wells/sinks) (Peuquet 1988), can be used as constraints on the generation of unstructured meshes. These data sets can be irregular or regular sample points, contours, polygons, grid cells and triangular nets. All these types of data sets can be handled as one of the three kinds of constraining layers (Bern and Eppstein 1992) in domain decomposition as discussed earlier:

5.2.1. Internal p*olygons/polylines*

Reprocessed internal polygons and polylines can serve as an internal boundary for triangulation which essentially means that they can support triangulation on either side of boundary. The triangulation generated while taking into account the polyline PSLGs as constraining boundaries is called a constrained Delaunay triangulation (CDT). Internal boundaries pose an extra constraint for Delaunay triangles as their interior can not intersect a boundary segment and their circumcircles should not encloses any vertex of the PSLG that is *visible* from the interior of the triangle (Shewchuk 1996). Two points are said to be visible to each other when no PSLG lies between them. CDT has been also used by Vivoni *et. al.* (2005) while using landscape indices as the PSLG. However, constrained Delaunay leaves some of the triangular elements adjacent to the PSLG to be non-delaunay. By the addition of extra Steiner points on the PSLGs, such triangles are transformed to follow a conformed Delaunay Triangulation property while still respecting the shape of the domain as well as the PSLG.

5.2.1.1. Typical internal polygons: Thematic classes and hydrodynamic descriptors. Examples of internal polygon boundaries are thematic classes like soil types and land use/land cover types or hydrodynamic descriptors like subshed boundaries and hypsometry.

The unique advantage of using thematic classes as constraints in decomposition is that the resulting model grid contains a single class. This leads to non-introduction of any additional data uncertainty arising from subgrid variability of themes within a model grid. Figure 11 highlights this concept, where an unstructured mesh generated using soil theme as a constraint leads to decomposition where each triangle has a single soil type. For structured grid decomposition with the same average resolution as the unstructured mesh, we observe that 41.63 % percent of the grids have mixed themes. Generating grids that do not follow edges of thematic classes (as shown in the case of structured grids) introduces uncertainty in parameterization and its effect is widely documented in hydrologic modeling literature (Beven 1995, Yu 2000).

Hydrodynamic descriptors can be thought of as topographic controls, such as subshed boundaries and hypsometry that influence the movement of water through the landscape (Winter 2001). Implementing hydrodynamic descriptors as constraints in domain decomposition (as shown in Figure 5) has several advantages in modeling:

1) Precise evaluation of the magnitude of groundwater flux exchanges across the subshed boundaries. Since the subshed topographic boundaries are fixed (and so are the mesh edges that are anchored to these boundaries), seasonal shifts in the ground water divide and flux with respect to the subshed boundaries can be tracked.

2) The specified no-flux condition on surface water flow across the subshed boundaries reduces computation load.

3) It is evident from Figure 5 that the triangular elements along the boundaries are smaller than internal elements. The subshed boundaries also represent relatively higher regions in the watershed where the hydrologic gradient can be expected to be high. Large gradients in elevation directly affect changes in temperature, wind, precipitation and vegetation. In order to capture these changes, relatively smaller sized meshing is needed. The approach to triangulation of subshed boundaries outlined above helps to achieve this.

4) This approach also provides an multi-scale framework of modeling the basin at watershed and subshed scales simultaneously.

Another hydrodynamic descriptor is hypsometry. Shun and Duffy, 1998 observed that a simple three-region hypsometric classification of watershed area into upland, lowland and middle elevation intervals could capture important elevation changes in precipitation-temperature-runoff. The uplands generally act as recharge zones, intermediate elevations as translational zones and lower regions as discharge zones. Hypsometry, or area – altitude relationship, relates horizontal cross- sectional area of a drainage basin to the relative elevation above base level (Strahler 1952). Strahler (1958) interpreted regions with low hypsometric values as eroded landscapes and high values as young landscapes with low erosion. This means that polygons corresponding to the three hypsometric divisions can be assigned unique attributes according to their characteristic time scales of groundwater flow or geomorphic evolution. Separating boundaries can be treated as contours. Figure 12 shows the hypsometric curve for Little Juniata Watershed. The three hypsometric divisions are obtained using the Jenks's optimal classification strategy (Coulson 1987 and Jenks 1977). With this method, intra-class variance of elevation values is minimized and the differences between classes are maximized resulting in better representation of groupings and patterns inherent in the dataset. As is evident from Figure 12 regions in the basin that are relatively flat have larger triangular elements whereas the mountainous regions are discretized into small elements. Traditional slope preserving meshes that retain high nodal density in regions of high terrain variability (Lee 1991) are generated when the constraints are derived from elevation.

5.2.1.2. Typical internal PSLGs: River network. An important example of constraining PSLGs used in domain decomposition is a river network. A higher concentration of triangles generated along the river network (see Figure 2) reflects the relatively faster hydrodynamics of riparian regions. Accurate assessment of flooded areas that get inundated with slight increase in river head can be performed when smaller triangles are generated in the vicinity of the river network. This facilitates flood-plain and flood inundation zone mapping.

We note that with the increasing number of internal boundary constraints, the number of mesh elements increases. This implies that a tradeoff exists between accuracy of representation of watershed properties (which is gained through the use of internal boundary constraints) and computational load. While the choice of any of these constraints is optional, any decision to insert an internal boundary must take into account the tradeoff between accuracy and computational load. Assuming that there is no uncertainty associated with the location of internal boundary itself, quantification of accuracy gained after the use of an internal boundary can be done at - a) "pre-modeling" stage, where accuracy in representation of a watershed property on decomposed domain is assessed, and b) "post-modeling" stage, where accuracy in representation of modeled physical states such as evapotranspiration, spatial distribution of snow etc. are assessed. For particular boundary types (like soil and vegetation), the uncertainty associated with their position and degree of transition can be significant. In such situations, representational accuracy calculations must be weighted by the inherent positional uncertainty. The error posed by such uncertainty can be limited to a certain extent by

using a buffer region (and the boundary) on the either side of the boundary as constraints. Buffer constraint will lead to generation of smaller mesh elements on the either side of the boundary until some specified width quantified by "position/transition-uncertainty". In such cases, mixed transition properties can be specified to the cells inside the buffer while using “hard” categorical properties outside of it.

5.2.2. Holes

The data structure of a hole is exactly that of a polygon. But there is a constraint on the operation. Holes are regions inside the basin boundary or other polygons that act as an external boundary and so are not triangulated. One example of a hole is a lake. Figure 13 shows the Great Salt Lake and Utah Lake within Great Salt Lake basin regions. Assuming the height of water in the lake is same everywhere within its boundary, the lake can be considered as a single control volume entity for modeling. This of course saves computational load where the assumption is valid. For a model scenario of increasing lake levels from a minimum pool, the adjacent elements will be submerged. However, because of the relatively small triangles adjacent to the boundary, a more accurate depiction of temporal changes in spatial extent of lake boundary and inundated areas can be performed.

5.2.3. Points:

Constraining points along with the Steiner points act as vertices for triangulation. A Steiner point is a node that is inserted in a line to divide it into smaller segments. It is not a part of the original set of constraining points and is generated only during triangulation. A typical constraining point can be the stage observation stations at hydraulic control structures like weirs, gates, pumps etc or ground water measuring stations. Modeled results of state variables at these constraining points can be compared directly to the observed values. This reduces any uncertainty in comparison of model results to observation as it happens in most cases where observation stations are not exactly the modeled locations. Figure 14 shows mesh decomposition for two cases, one with observation stations as constraint and the other without it. We note that the observation station on the river, as well as in the watershed is left to dangle somewhere in the middle of the discretized element in the unconstrained decomposition case. For comparison with stage or groundwater level obtained from the model in such cases will need interpolation of modeled results to observation locations. On the other hand in a constrained decomposition case, observation stations can also act as a node for triangulation resulting in simulation of state variables exactly at the modeled locations. To put it simply, modeled location and observation locations are the same in the constrained decomposition case. In the future, constrained domain decomposition based on the sensor-networks locations should facilitate direct assimilation of observed data into the model (Reed et. al. 2006)

6. Advances in hydrologic modeling

Using the constrained decompositions discussed earlier, integrated modeling of hydrologic processes in Little Juniata Watershed (shown in Figure 2) is performed. For detailed model related information, readers are referred to Kumar *et. al.* 2008. The model generates a large amount of spatio-temporal data of each hydrologic state such as interception storage, snow depth, overland flow, ground water depth, soil moisture, river flow and evapotranspiration. Figure 15 shows a representative spatial distribution of modeled evapo-transpiration at two snapshots in time. We also show the spatial distribution of average river streamflow, percentage of time different sections of the river is gaining and finally the streamflow time series at four separate locations in the watershed. These are few of the spatio-temporal predictions obtained from model simulation. The model results shown in Figure 15 are from a static decomposition of the watershed. A higher resolution modeling with least additional computational burden can be performed by a) selective "zooming" in an area of interest while leaving discretization in rest of the watershed to be coarse, and b) adaptively changing the grid resolutions in different parts of the watershed depending on the spatial rate of change of a physical state in a localized region.

Such advanced modeling is facilitated by the flexibility in generation of multi-resolution nested and adaptive (refinement/derefinement) unstructured meshes while using different constraints.

6.1. Nested triangulation

Nested models are already common in other fields of science, (e.g. fluid dynamics: Carey *et al.* 2003, geology: Gautier *et. al.* 1999; and climatology: Loaiciga *et. al.* 1996). In hydrologic modeling, development of nested models is still in its infancy stage (Grayson and Blöschl 2001). The basic principle behind this strategy is triangulation of the domain of interest into large elements combined with locally refined or nested grids where higher resolution is necessary. The main advantage of the approach is seamless assimilation of spatially varied forcings, parameters or the constitutive relationships in different regions of the basin. This nested-grid configuration makes it possible to combine realistic large-scale simulations with mesoscale forecasts for selected regions. Figure 16 shows that triangles generated in a subshed around the main stem of Little Juniata River are much smaller than the rest of the basin. This local high-resolution representation of parameters and processes minimizes computation. Nested triangulations will have applications for:

1) integrated hydrologic studies in larger basins which have high resolution data-support in one of its subwatersheds. The subwatershed in this case can be decomposed at relatively higher resolution than the rest of the basin to take maximum advantage of the high resolution observed data while still maintaining all boundary conditions and conservation rules.

2) studies which focus on understanding scaling issues and comparison of scaling effects across the basin.

3) the implementation of new physical processes in watershed and river basin studies which are relatively more computationally intensive. One example might be physics - based snows melt modeling. Modeling snow-melt is quite critical in mountainous basins as it directly affects flooding, contaminant transport, water supply recharge and erosion (Walter *et. al.* 2005). Snow-melt modeling generally falls in two categories: *temperature-*

index models that assume an empirical relationship between air temperature and melt rates and *energy- balance* models that quantifies the melt amount by solving energy balance equations. The most common justification for temperature index snowmelt models is the need for a reduced number of input variables, and also the model and computational simplicity. Several researchers (Ambroise et al. 1996, Fontaine et al. 2002) have derived acceptable results from temperature index models. Nevertheless, because of the incorporation of energy interaction between topography, wind and radiation, an energy-balance model is better placed in simulation of spatial heterogeneity in snow accumulation and redistribution (Winstral and Marks 2002). Since, energy based models like SNOBAL (Marks et al. 1998) run at shorter time intervals, need a high resolution DEM and forcing data as its support and solves a large number of state variables; they can only be run over a small watershed with present computational constraints or run in an offline weakly coupled mode. So an energy based modeling can be performed in the high resolution nested watershed while temperature-index modeling approach can be used for rest of the watershed.

4) watersheds susceptible to large and frequent floods in limited areas but where the runoff is generated in upland non-flooding areas. Higher resolution discretization in a watershed will lead to accurate mapping of areas which will get flooded with given increase in stream-stage level (Shamsi 2002).

5) understanding the relation of groundwater flow dynamics within a subshed to the rest of the basin. Subshed topographic boundaries are simply a surface descriptor and as noted by Brachet 2005, the groundwater flow divide can change seasonally affecting the water flux in and out of the watershed. With a nested modeling approach, movement of ground water divide can be mapped with acceptable precision.

Clearly the nested triangulation strategy has implications for studying the scaling behavior and scale transitions with a river basin.

6.2. Adaptive refinement/derefinement of triangulation

The triangulation and domain representation discussed above, is spatially adaptive in the sense that the resolution of the elements are not uniform. The resolution and distribution of triangles depends on the constraining layers, the tolerance in VIP generation and the polyline reconditioning algorithms, and the boundary heterogeneities. Clearly, widely varying spatial and temporal scales, in addition to the nonlinearity of the dynamical system can raise interesting and challenging modeling problems. In many applications, because of the particular dynamics of the problem, meshes may need to be further (de)refined locally after initial computation. An example is when the computed solution is rapidly varying in time within small areas of the domain while the solution is relatively slow in other parts. Solving such a problem more efficiently and accurately requires a solution-adaptive triangulation strategy. This is a necessity for resolving coupled physics with different time scales which is encountered in hydrologic models. Solution adaptation can save several orders of magnitude in computational load by avoiding under-resolving high-gradient regions in the problem, or conversely, over resolving low gradient regions at the expense of more critical regions. While this strategy can prove problematic within finite difference and finite element analyses, finite volume

methods, particularly those based on a triangular mesh system, lend themselves quite naturally to automatic adaptive refinement/de-refinement procedures (Sleigh et. al. 1995).

Dynamically adaptive grid approaches have long been used in astrophysical, aeronautical and other areas of computational fluid dynamics problems (Berger and Oliger 1984, Berger and Colella 1989). Zhao *et. al.* (1994) used a Riemann solver approach to calculate fluxes on unstructured, mixed quadrilateral-triangular grid system in river and flood plain. Sleigh et. al. (1998) used adaptive refinement/de-refinement for computational efficiency while predicting flow in river and estuaries using unstructured finite volume algorithm. For a finite volume integrated hydrologic model like PIHM, adaptive refinement can be carried out in the regions where intermittent dynamics occurs. An example is an ephemeral channel. Since the channel is dry for most part of the year, there is no need to have an *a priori* high-resolution grid. Depending on the status of the channel network, the dynamics will trigger adaptive refinement/de-refinement. Other situations include hortonian runoff, convective precipitation in a part of basin and sudden increase in river stage due to dam break or flash floods. In each case adaptive refinement/de-refinement of existing triangulations will save on the computation load. Figure 17 shows the flow diagram depicting the refinement/de-refinement procedure. Refinement is performed by inserting carefully placed vertices until the triangular element meets constraints on element quality and size which is decided *a priori*. Inserting a vertex to improve elements that don't satisfy the refinement criterion in one part of a mesh will not unnecessarily perturb a distant part of the mesh that has no "bad" elements. That is, insertion of a vertex is a local operation, and hence is inexpensive except in unusual cases. The refinement/de-refinement criterion is generally based on metrics that quantify a sudden change in magnitude of a state variable over a localized area or time. Figure 18 shows refinement of two marked triangles in different parts of domain. It is obvious from the figure that the original triangulation is affected locally only.

7. Conclusion

A strategy for unstructured mesh decomposition is proposed which captures the phenomenological and hydrologic complexity of the watershed while minimizing the equations to be solved. The framework provides a tight coupling between geo-data and the processes that are modeled on it. The strategy seamlessly incorporates computational geometry based algorithms to process GIS feature objects for discretization for model domain. The framework incroporates the constraints posed by hydrologic process dynamics, numerical solver, data heterogenity and computational load. It outperforms structured grids based representations in terms of accurate representation of raster and vector layers. Polygon reprocessing and polyline reconditioning algorithms facilitate the use of available GIS feature objects in domain decomposition. Flexibility of the framework in terms of model implementation, model development, data and process constraints, and elevation-derived-VIPs, provides added advantages when compared to traditional TINs. Rapid prototyping of meshes which better reflect the constraints of the problem under consideration can be obtained. The problem constraints that are addressed include: the computational burden, the need for reduction in uncertainty of state variables, the accurate specification of boundary conditions, the application of multiscale or nested models, and the need for dynamically adaptive refinement/de-refinement.

In summary, the "support-based" domain decomposition and unstructured grid framework provides a close linkage between geo-scientific data and complex numerical models. The strategy extends the GIS based algorithms to be used in distributed numerical modeling setting. The framework is generic and can be implemented for linking other numerical process models of mass, momentum and energy to their respective geodatabases.

References

ABBOT, M.B., BATHURST, J.C., CUNGE, J.A., O'CONNELL, P.E. and RASMUSSEN, J. 1986, An Introduction to the European Hydrological System – Systeme Hydrologique Europeen, "SHE", 2 : History and Philosophy of a Physically-based, Distributed Modelling System. *Journal of Hydrology*, 87, 61-77

AMBROISE, B., FREER, J., BEVEN, K.J., 1996. Application of a generalised TOPMODEL to the small Ringelbach catchment, Vosges, France. *Water Resources Research*, 32, 2147–2159.

BAKER B.S., GROSSE E., and RAFFERTY, C.S., 1988. Nonobtuse triangulation of polygons. *Discrete and Computational Geometry*, 3, 147-168.

BAND, L. E., 1986. Topographic partition of watersheds with digital elevation models. *Water Resources Research*, 23(1), 15–24.

BERGER, M. J., and COLELLA, P., 1989. Local adaptive mesh refinement for shock hydrodynamics. *Journal of Computational Physics*, *82* (1), 64–84.

BERGER, M., and OLIGER, J., 1984. Adaptive mesh refinement for hyperbolic partial differential equations. *Journal of Computational Physics*, 53 , 484–512.

BERN, M.W., EPPSTEIN, D., 1992. Mesh Generation and Optimal Triangulation, *Computing in Euclidean Geometry: Lecture notes on computing, World Scientific*, 23-90.

BERN, M., MITCHELL, S., and RUPPERT, J., 1994. Linear-size nonobtuse triangulation of polygons. In *Proceedings of 10th ACM Symposium on Computational Geometry*, 221-230.

BEVEN K.J., 1995. Linking Parameters Across Scales: Subgrid Parameterizations and Scale Dependent Hydrological Models. *Scale Issues in Hydrological Modelling*, Kalma, J.D., Sivapalan M. (eds); Wiley: Chichester, pp. 263-281.

BLAYO, E., and L. DEBREU, 1999. Adaptive mesh refinement for finite difference ocean model: some first experiments. *Journal of Physical Oceanography*, 29, 6, 1239-1250.

BRAUN, J., and SAMBRIDGE, M., 1997, Modelling landscape evolution on geological time scales: a new method based on irregular spatial discretization. *Basin Research*, 9, p. 27-52.

CAREY, G., KIRK B. and LIPNIKOV, K, 2003. Nested grid iteration for incompressible viscous flow and transport. *International Journal of Computational Fluid Dynamics*, 17(4):253-262

CASTILLO, J.E. (Eds.), 1999. Mathematical Aspects of Numerical Grid Generation. SIAM, Philadelphia.

CHEW, L.P., 1993. Guaranteed-Quality Mesh Generation for Curved Surfaces. In *Proceedings of the Ninth Annual Symposium on Computational Geometry* (San Diego, California), pages 274–280. Association for Computing Machinery

COULSON, M.R.C., 1987, In the matter of class intervals for choropleth maps: With particular reference to the work of George F. Jenks: *Cartographica*, 24, p. 16-39

COURANT, R., FRIEDRICHS, K.O., LEWY, H., 1928. Uber die partiellen differenzgleichungen der mathematischen physic (on the partial difference equations of mathematical physics). *Mathematische Annalen* 100, 32–74.

DOUGLAS, D., PEUCKER, T., 1973. Algorithms for the reduction of the number of points required to represent a digitized line or its caricature. *The Canadian Cartographer* 10, 112–122.

ENTEKHABI, D., and EAGLESON, P.S., 1989. Land surface hydrology parameterization for atmospheric general circulation model including subgrid scale spatial variability. *Journal of Climate*, 2, 816-831.

FAIRBANKS, J., PANDAY, S., and HUYAKORN, P.S., 2001. Comparisons of linked and fully coupled approaches to simulating conjunctive surface/ subsurface flow and their interactions. In Seo, Poeter, Zheng, Poeter, (Eds). MODFLOW 2001 and Other Modeling Odysseys— Conference Proceedings, Golden, CO;p. 356–61

FONTAINE, T.A., CRUICKSHANK, T.S., ARNOLD, J.G., HOTCHKISS, R.H., 2002. Development of a snowfall-snowmelt routine for mountainous terrain for the soil water assessment tool (SWAT). *Journal of Hydrology* 262, 209–223.

GAUTIER, Y, BLUNT, M.J., CHRISTIE, M.A., 1999. Nested gridding and streamline based simulation for fast reservoir performance prediction. *Computational Geosciences* 3:295-320

GOODRICH, D.C., 1990. Geometric simplification of distributed rainfall-runoff model over a range of basin scales. PhD Dissertation, Tucson, AZ: Department of Hydrology and Water Resources, University of Arizona, 361 pp.

HENRY, R.F., WALTERS, R.A., 1993. Geometrically based, automatic generator for irregular triangular networks. *Communications in Numerical Methods in Engineering* 9 (7), 555–566.

GRAYSON, R. and BLÖSCHL, G. 2001. *Spatial patterns in catchment hydrology*. Cambridge University Press.

IVANOV, V.Y., VIVONI, E.R., BRAS, R.L. and ENTEKHABI, D., 2004. Catchment hydrologic response with a fully-distributed triangulated irregular network model. *Water Resources Research*, 40.

HITSCHFELD, N., RIVARA, M.C, 2002, Automatic construction of non-obtuse boundary and/or interface delaunay triangulations for control volume methods, *International Journal of Numerical Methods in Engineering*, 55,803-816.

JENKS, G.F. 1977. Optimal data classification for choropleth maps. Occasional paper No. 2, Department of geography, University of Kansas, Lawrence.

JONES, N.L., WRIGHT, S.G., and MAIDMENT, D.R., 1990. Watershed delineation with triangle based terrain models. *Journal of Hydraulic Engineering* 116:1232-1251

KUMAR, M., BHATT, G. and DUFFY, C., 2008. Role of process and data coupling in Mesoscale Watershed Model, *Advances in Water Resources* (in review)

KOLLET, S. J., and MAXWELL, R. M., 2006, Integrated surface-groundwater flow modeling: A free-surface overland flow boundary condition in a parallel groundwater flow model, *Advances in Water Resources*, (29)7, 945-958

LEE, J., 1991. Comparison of existing methods for building triangular irregular network models of terrain from grid digital elevation models. *International Journal of Geographical Information Systems*, 5(3), pp. 267–285.

LOAICIGA, H.A., VALDES, J.B., VOGEL, R., GARVEY, J., SCHWARZ, H., 1996. Global warming and the hydrologic cycle. *Journal of Hydrology* 174:83-127

MAIDMENT, D.R. (Ed.), 2002, Arc Hydro: GIS for Water Resources (Redlands, CA: ESRI Press, 2002).

MARKS, D., KIMBALL, J., TINGEY, D., LINK, T., 1998. The sensitivity of snowmelt processes to climate conditions and forest cover during rain-on-snow: A study of the 1996 Pacific Northwest flood. *Hydrological Processes* 12: 1569-1587.

MILLER, G.L., TALMOR, D., TENG, S.H., and WALKINGTON, N., 1995. A Delaunay Based Numerical Method for Three Dimensions: Generation, Formulation, and Partition. In *Proceedings of the Twenty- Seventh Annual ACM Symposium on the Theory of Computing* (Las Vegas, Nevada), pages 683–692.

MOORE I. D., O'LOUGHLIN, E.M., BURCH. A., 1988. Contour-based topographic model for hydrological and ecological applications, *Earth Surface Processes Landforms*,13,305-320.

NYERGES, T.L., 1993. Understanding the scope of GIS: Its relationship to environmental modeling. In *Environmental Modeling with GIS*, Goodchild, M.F., Parks, B.O. and Steyaert, T. (Eds.), New York: Oxford University Press, pp. 75-93.

PANDAY, S., and P.S. HUYAKORN, 2004. A fully coupled physically-based spatially-distributed model for evaluating surface/subsurface flow, *Advances in Water Resources*, 27, 361-382.

PEUQUET, D.J., 1988, Representations of geographic space: Towards a conceptual synthesis. *Annals of the Association of American Geographers*, 78, pp. 375-394.

PITMAN, A.J., HENDERSON-SELLERS, A., and YANG, Z.L., 1990. Sensitivity of regional climates to localised precipitation in global models. *Nature*, 346, 734-737.

REED, P. M., BROOKS, R. B., DAVIS, K. J., DEWALLE, D. R., DRESSLER, K. A., DUFFY, C. J., LIN, H., MILLER, D. A., NAJJAR, R. G., SALVAGE, K. M., WAGENER, T., and YARNAL, B., 2006. "Bridging River Basin Scales and Processes to Assess Human-Climate Impacts and the Terrestrial Hydrologic System." Part of CUAHSI/NSF Hydrologic 4 Vision Series, *Water Resources Research*, 42.

RUPPERT, J. 1995. A Delaunay Refinement Algorithm for Quality 2-Dimensional Mesh Generation. *Journal of Algorithms*, 18(3):548–585.

SHUN.T., and DUFFY, C.J.,1998. Low-frequency oscillations in precipitation, temperature, and runoff on a west facing mountain front: A hydrogeologic interpretation, *Water Resources Research*.,35,191-201

STRAHLER, A.N., 1952. Hypsometric (area-altitude) analysis of erosional topography. *Geological Society of America Bulletin*, 64:165-176.

STRAHLER, A.N., 1958. Dimensional analysis applied to fluvially eroded landforms, *Geological Society of America Bulletin*, 69, 279-300.

SHAMSI, S.U., 2002, GIS applications in floodplain management, In *ESRI GIS user conference*, Tel Aviv.

SHEWCHUK, J.R., 1997. Delaunay refinement mesh generation, PhD Thesis, Carnegie Mellon University.

SHEWCHUK, J.R., 1996. Triangle: Engineering a 2D quality mesh generator and Delaunay Triangulator. In *1st workshop on Applied Computational Geometry*, ACM, 124-133.

SLEIGH, P. A., GASKELL, P. H., BERZINS, M., WARE, J. L. and Wright, N. G., 1995. A reliable and accurate technique for the modelling of practically occuring open channel flow. In *Proceedings of the Ninth International Conference on Numerical Methods in Laminar and Turbulent Flow*, 881-892.

SLEIGH, P. A., GASKELL, P. H., BERZINS, M., WARE, J. L. and Wright, N. G., 1998. An unstructured finite volume algorithm for predicting flow in rivers and estuaries. *Computer and Fluids*, Vol. 27, 4, 479-508.

TARBOTON, D.G., 1997, A new method for the determination of flow directions and contributing areas in grid digital elevation models. *Water Resources Research*, 33, no. 2, p. 309-319.

TARBOTON, D. G., and D. AMES. 2001. Terrain Analysis Using Digital Elevation Models. In *Forest Service 2001 Geospatial Conference*, Salt Lake City.

THOMPSON, J.F., (Eds.), 1982. *Numerical Grid Generation*. North-Holland

VAVASIS, S.A., 1993. Stable finite elements for problems with wild coefficients. Tech. Report TR93-1364, Dept. of Comp. Science, Cornell University.

VIVONI E.R., IVANOV, V.Y., BRAS, R.L. and ENTEKHABI, D., 2004. Generation of triangulated irregular networks based on hydrological similarity. *Journal of hydrologic engineering*, 9, 4. 288-302.

VIVONI, E.R., TELES, V., IVANOV, V.Y, BRAS, R.L., and ENTEKHABI, D., 2005. Embedding landscape processes into triangulated terrain models. *International Journal of Geographical Information science*, Vol. 0, No. 0, 1-29.

WALTER, M.T, BROOKS, E.S., MCKOOL, D.K., KING, L.G., MOLNAU, M., and BOLL.J., 2005. Process based snowmelt modeling: does it require more input data than temperature-index modeling? *Journal of Hydrology*, 65-75.

WEATHERILL, N. P., 1998, Introduction to Unstructured Grids in Handbook of Grid Generation, Thompson, J. F., Soni, B. K., and Weatherill, N. P. (Eds.), CRC Press.

WINSTRAL, A. and MARKS, D. 2002. Simulating wind fields and snow redistribution using terrain- based parameters to model snow accumulation and melt over a semi-arid mountain catchment, *Hydrologic Processes*, 16, 3585-3603.

WINTER, T.C., 2001, The concept of hydrologic landscapes. *Journal of the American Water Resources Association*, 37, p. 335-349.

WOO., M.K, 2004. Boundary and border considerations in hydrology, *Hydrological Processes*, 18, 1185-1194.

YU, Z., 2000. Assessing the response of subgrid hydrologic processes to atmospheric forcing with a hydrologic model system. *Global Planet Change*, 25, pp. 1–17

ZHAO, D.H., SHEN, H.W., TABIOS, G.Q., LAI, J.S. and TAN, W.Y., 1994. Finite-volume Two-dimensional Unsteady-flow Model for River Basins, *Journal of Hydraulic Engineering*, 120(7), 863–883.

Figures

Figure 1: Domain decomposition of Little Juniata Watershed using rectangular grid. The "zoomed in" portion of the boundary shows aliasing (stair-case effect) of watershed boundary by structured mesh. Such aliasing can be expected near all kinds of topographic, hydrographic (river, lakes etc.) and physiographic (land use/land cover, soil types etc.) boundaries.

Figure. 2: All the interacting hydrologic processes in PIHM are defined on prismatic watershed elements or linear river elements. ODEs corresponding to each process from all across the model domain are solved together to predict state variables at next time step.

Figure 3: Data structure of Node, Polyline and Polygon feature objects. NumSeg ≡Number of line segments in a polyline. Seg. ID ≡ Line segment ID. NumPolyL ≡Number of Polylines. PolyL. ID ≡ Polyline ID.

Figure. 4: Intermediate steps in polygon to polyline simplification.

Figure 5: Bottom left and right figures show unstructured mesh decomposition of Little Juniata Watershed before and after reconditioning of polyline. Bottom two figures show the zoomed-in fused image of triangulations at two different locations in the watershed. Note the excessive high concentration of triangles formed in the "un-conditioned" case. Polyline reconditioning removes aliasing in the boundaries by removing nodes at unwanted locations.

Fig. 6: Intermediate steps in polyline simplification using Douglas-Peucker algorithm.

Figure 7: The number of mesh elements increases with increasing number of VIPs inserted during Delaunay triangulation and the decreasing tolerance magnitude used in polyline reconditioning of boundaries.

Figure 8: (a) Root mean square error in representation of DEM and Slope at three levels of mesh decomposition. Note, Decomposition Level –a,b and c- are same as those shown in Fig. 7. Structured grids based decomposition leads to larger error in both DEM and Slope representation than Unstructured grids. (b) Root mean square error in representation of polyline per unit length of polyline. At all decomposition levels, unstructured grids agree to the boundaries better than structured grids. Note: SrG ≡ Structured Grid Decomposition, UnSrG ≡ UnStructured Grid Decomposition

Figure 9: Circumcenter O of ΔABC will lie inside its boundaries if and only if the triangle is acute angled i.e. $\alpha < 90$.

Figure 10: The upper bound on *M* (ratio of circumradius to smallest triangular edge) is controlled inversely by an angle α that is subtended by the smallest side AB of the triangular element on the opposite vertex.

Figure 11: Top left unstructured mesh decomposition (UnSrG) is generated based on thematic class (soil type) boundary as constraint. Top right structured mesh (SrG) decomposition has same spatial resolution as the grid on left. Colored grid in the background of both the decompositions is a soil type map. The zoomed-in image shows that SrG (in light grey) have multiple soil classes within them. UnSrG edges (in red or dark grey (in black and white)) overlap soil class edges thus resulting in a "one soil class assignment" to each triangle

Figure 12: Left figure shows the elevation hypsometric curve of Little Juniata Watershed. Delaunay Triangulation of Little Juniata Watershed while using hypsometric division as a constraint. Expectedly in regions of higher topographic extremes/gradient, concentration of meshes is higher. Note the formation of smaller triangles besides the streams. Similar divisional constraints can be used for vegetation and climate regimes.

Figure 13: Domain decomposition of Great Salt Lake Basin. Note that no triangles are created inside the lake.

Figure 14: (a) Zoom-in of mesh decomposition with and without using groundwater observation stations as constraints for two locations inside the watershed (b) Mesh decomposition with (right side, green) and without (left side, grey) using observation stations as constraints (c) Zoom-in of mesh decomposition with and without using stage observation stations as constraints for two locations on Little Juniata River. We note that in constrained decomposition, triangulations are generated such that the observation stations lie directly on the mesh nodes.

Figure 15: (a) shows the average evapo-transpiration (ET) time series for the Little Juniata watershed for two year period. Snapshots for spatial distribution of ET during the maximum and minimum extremes are shown in (b) and (c) respectively. Since we have used same color range to represent both extremes, ET appears to be uniform everywhere (though that is not the case) during winter as the values are quite small. (d) and (e) shows the streamflow hydrograph at four locations in the stream network. (f) shows the percentage of time each stream segment gains water from the aquifer. We note that all the results shown above are for a simulation period of 2 years ranging from Nov, 1983 to Oct. 1985.

Figure 16: Nested Mesh decomposition of Little Juniata Watershed while using subsheds as internal boundary. For computational efficiency a localized region of the basin (around main stem of Little Juniata River, shaded in the figure) can be discretized to higher spatial resolution elements while leaving rest of the basin at coarser resolution. Under a single framework, mesoscale to microscale modeling can be performed.

Figure 17: Flow chart depicting the dynamically adaptive refinement/de-refinement algorithm for hydrologic modeling. Depending on the hydrodynamics, a particular region can be refined to finer or coarse triangular elements in order to capture the hydrologic process accurately.

Figure 18: Coarse-scale unstructured mesh decomposition of Little Juniata Watershed (Left). At any time *t* during simulation, two triangles (light grey) are marked as Bad Elements depending on spatial gradient estimate of a state variable and are identified for refinement. Decomposition on the right shows insertion of a node inside the marked elements and the resulting perturbed region. Note the formation of new triangles and the triangulated area that gets perturbed is very small relative to the whole watershed. Triangles in the unperturbed region remain same.

Figure 1: Domain decomposition of Little Juniata Watershed using rectangular grid. The "zoomed in" portion of the boundary shows aliasing (stair-case effect) of watershed boundary by structured mesh. Such aliasing can be expected near all kinds of topographic, hydrographic (river, lakes etc.) and physiographic (land use/land cover, soil types etc.) boundaries.

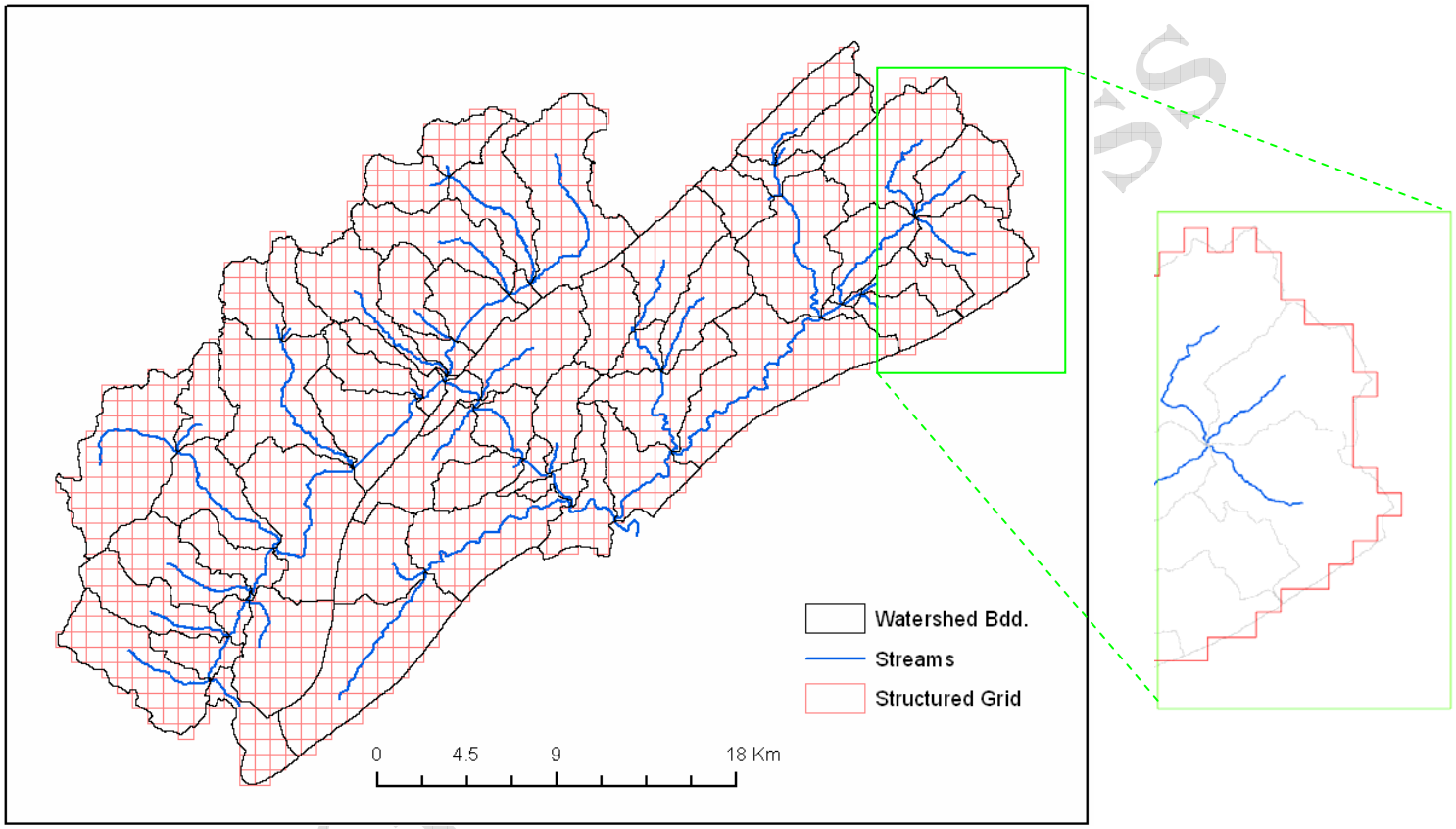

Figure. 2: All the interacting hydrologic processes in PIHM are defined on prismatic watershed elements or linear river elements. ODEs corresponding to each process from all across the model domain are solved together to predict state variables at next time step.

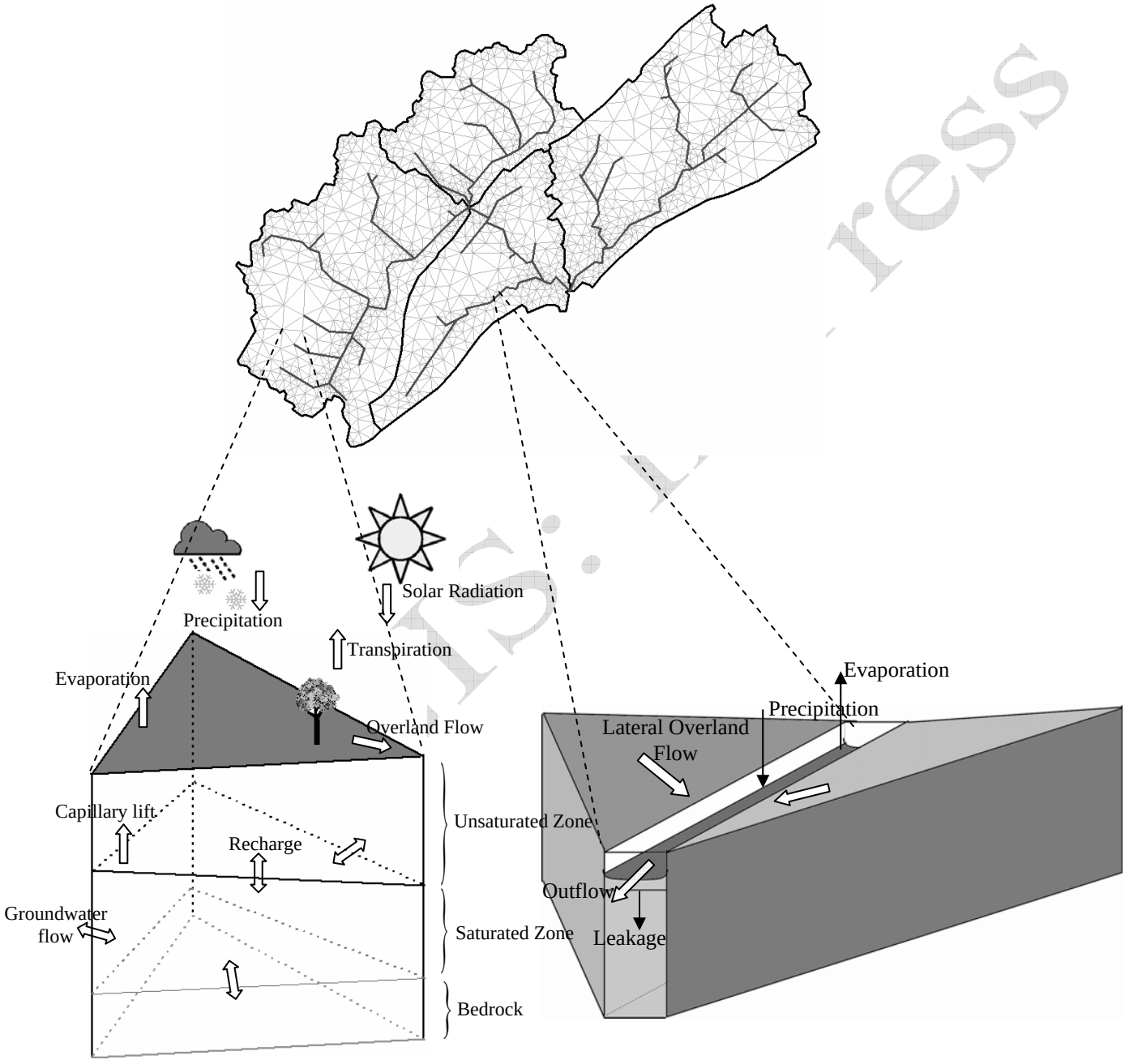

Figure 3: Data structure of Node, Polyline and Polygon feature objects. NumSeg ≡Number of line segments in a polyline. Seg. ID ≡ Line segment ID. NumPolyL ≡Number of Polylines. PolyL. ID ≡ Polyline ID.

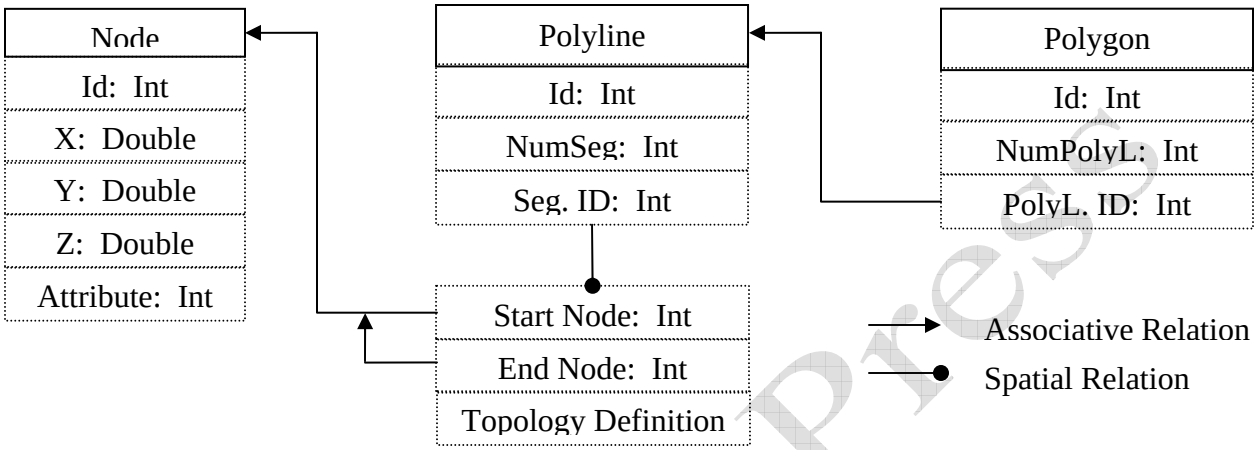

Figure. 4: Intermediate steps in polygon to polyline simplification.

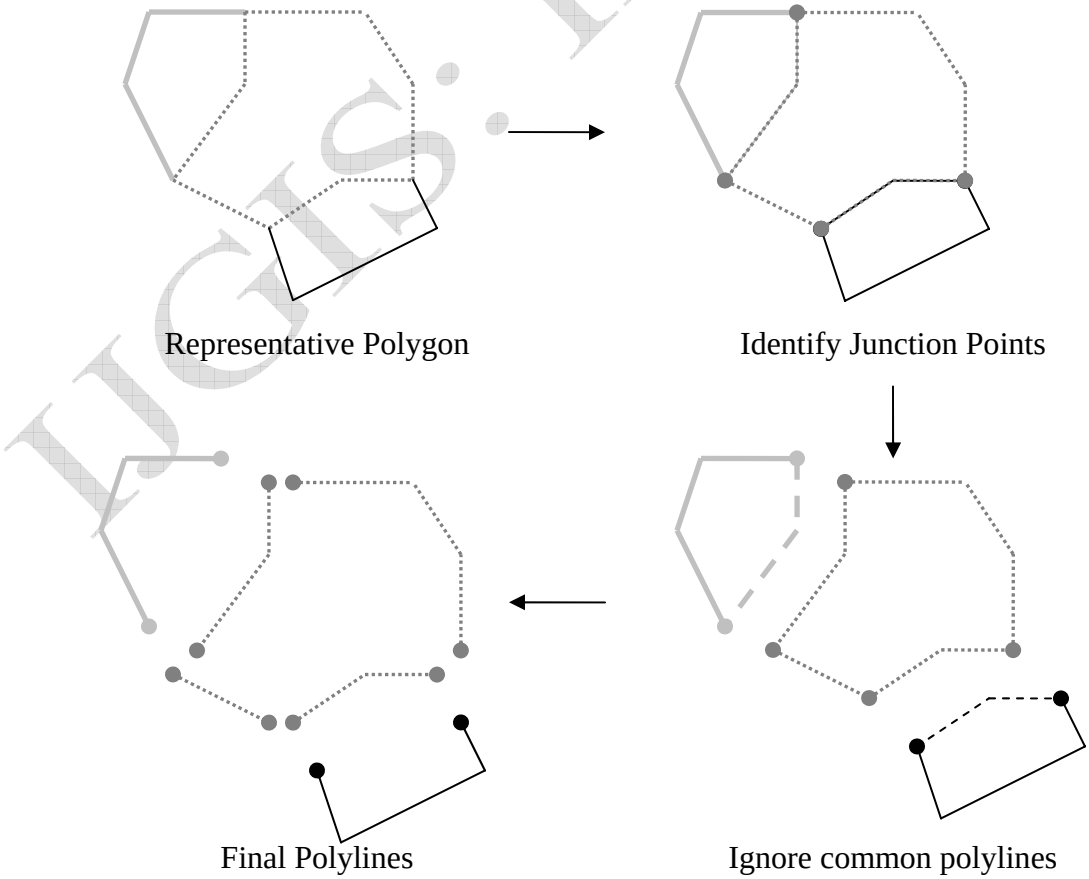

Figure 5: Bottom left and right figures show unstructured mesh decomposition of Little Juniata Watershed before and after reconditioning of polyline. Bottom two figures show the zoomed-in fused image of triangulations at two different locations in the watershed. Note the excessive high concentration of triangles formed in the “un-conditioned” case. Polyline reconditioning removes aliasing in the boundaries by removing nodes at unwanted locations.

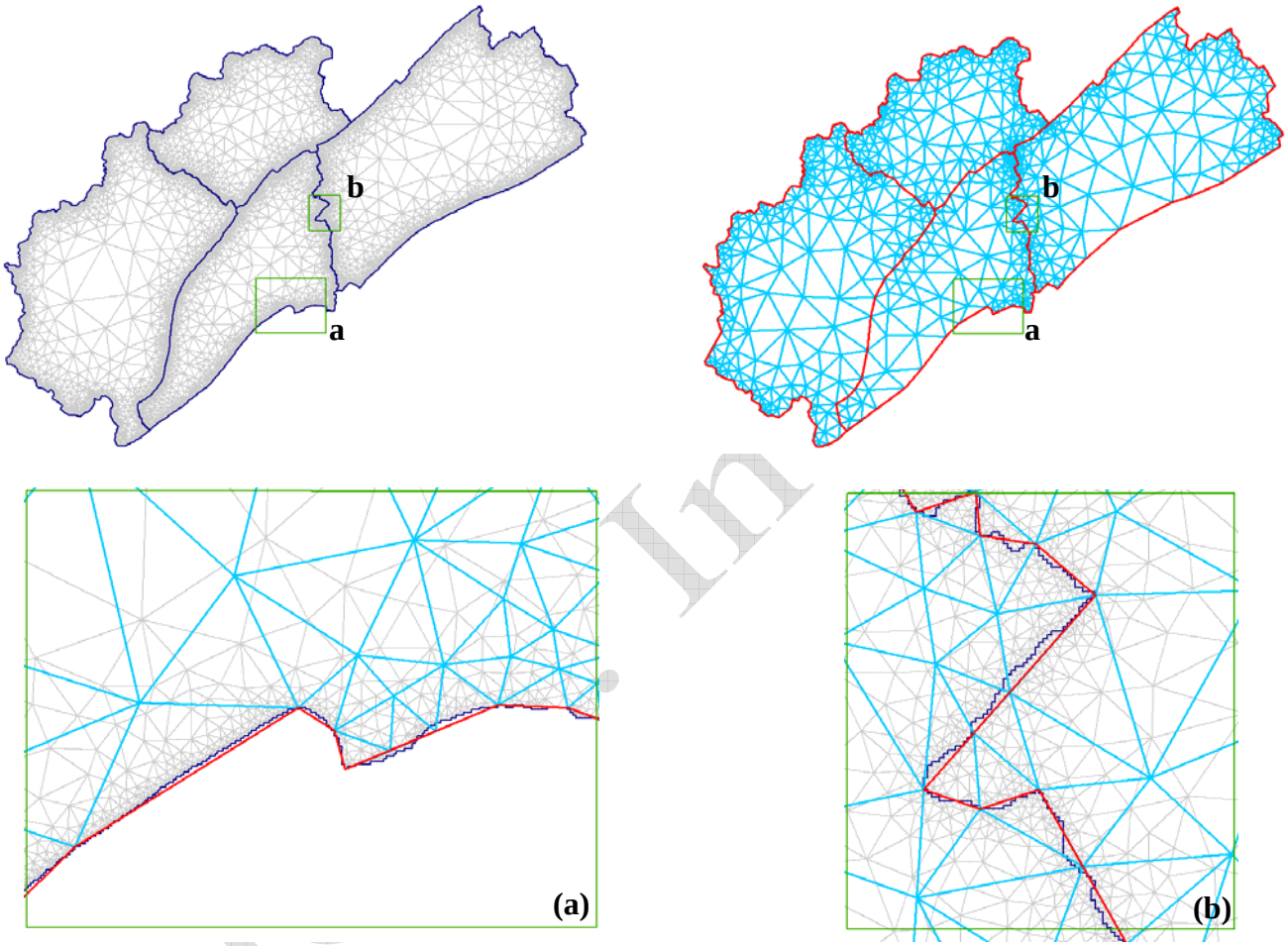

Fig. 6: Intermediate steps in polyline simplification using Douglas-Peucker algorithm.

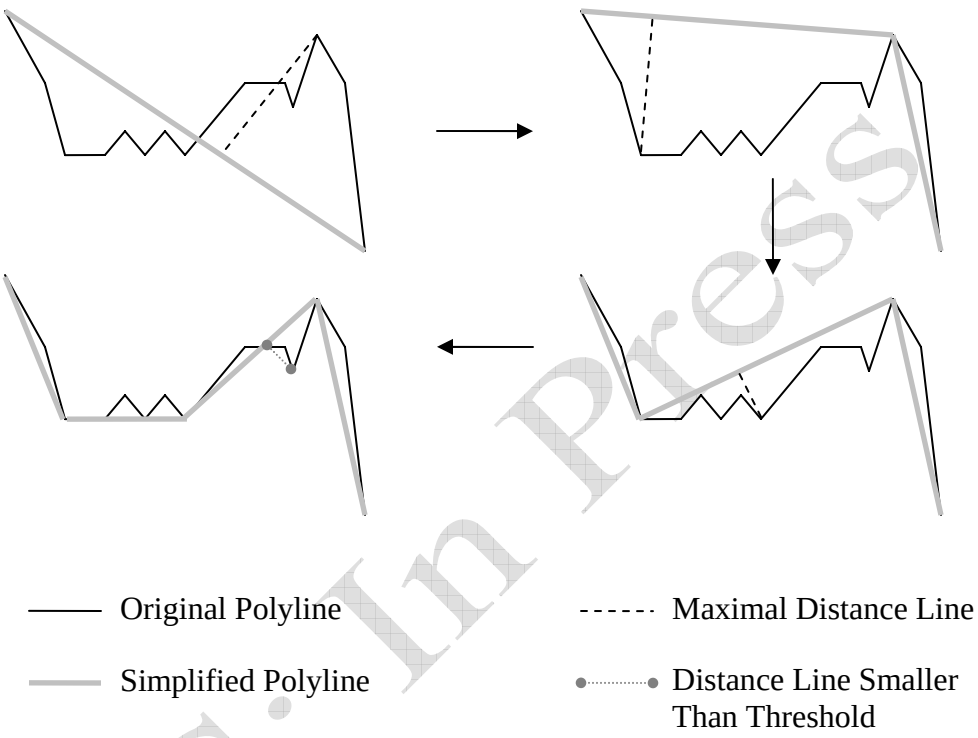

Figure 7: The number of mesh elements increases with increasing number of VIPs inserted during Delaunay triangulation and the decreasing tolerance magnitude used in polyline reconditioning of boundaries.

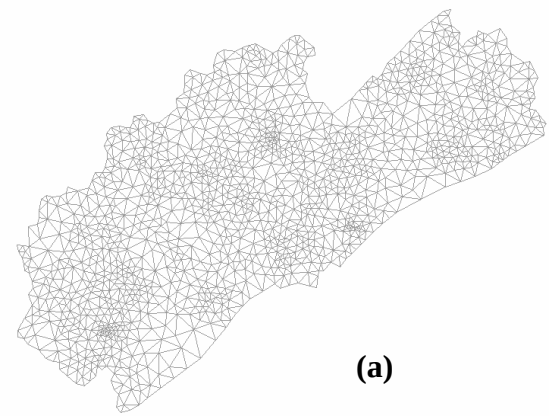

(a)

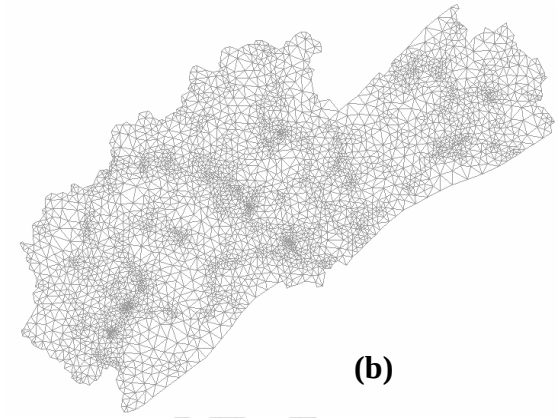

(b)

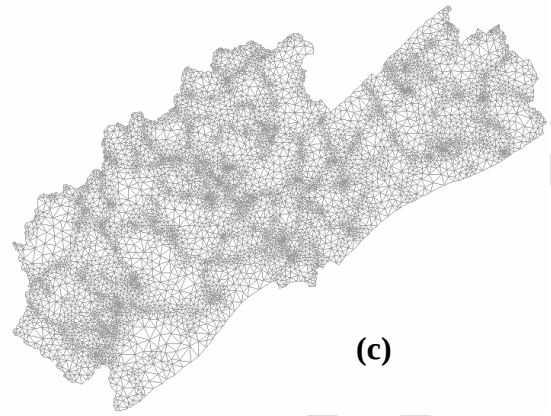

(c)

DL*	VIPs*	PT*	MN*	R_{sg}*
a	645	250	1448	770
b	1090	100	3386	503
c	1997	100	7326	342

* DL ≡ Decomposition Level
VIPs ≡ No. of Very Important points
PT ≡ Polyline Reconditioning Tolerance
MN ≡ No. of Mesh Nodes
R_{sg} ≡ Average structured grid resolution

Figure 8(a): Root mean square error in representation of DEM and Slope at three levels of mesh decomposition. Note, Decomposition Level –a,b and c- are same as those shown in Fig. 7. Structured grids based decomposition leads to larger error in both DEM and Slope representation than Unstructured grids.

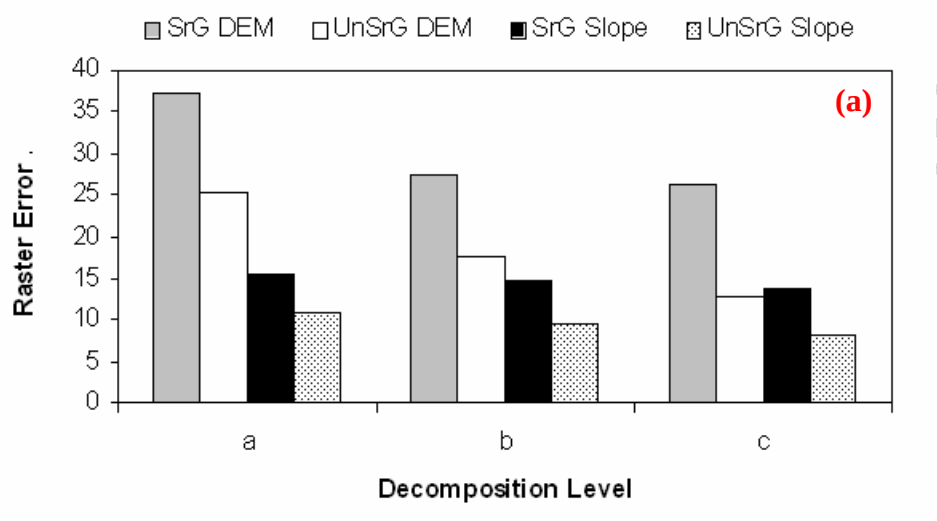

Figure 8(b) Root mean square error in representation of polyline per unit length of polyline. At all decomposition levels, unstructured grids agree to the boundaries better than structured grids. Note: SrG ≡ Structured Grid Decomposition, UnSrG ≡ UnStructured Grid Decomposition

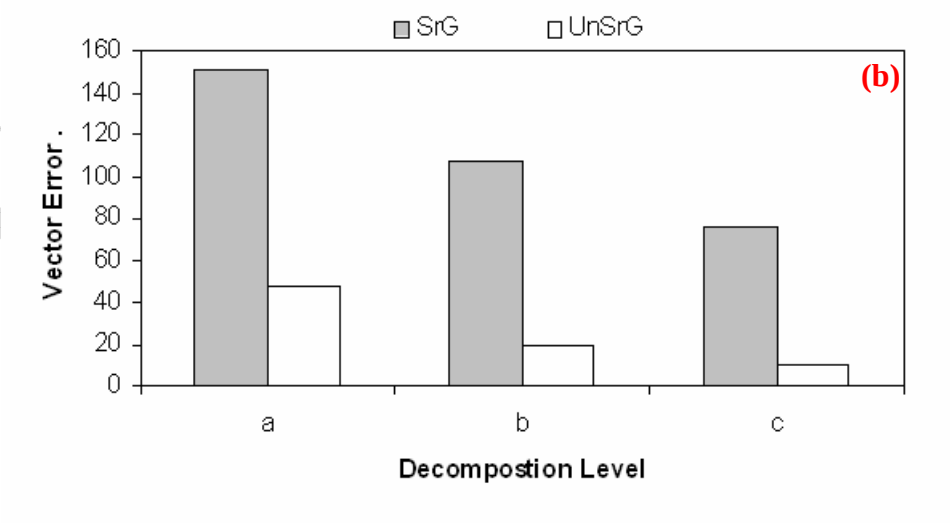

Figure 9: Circumcenter O of ΔABC will lie inside its boundaries if and only if the triangle is acute angled i.e. $\alpha < 90$.

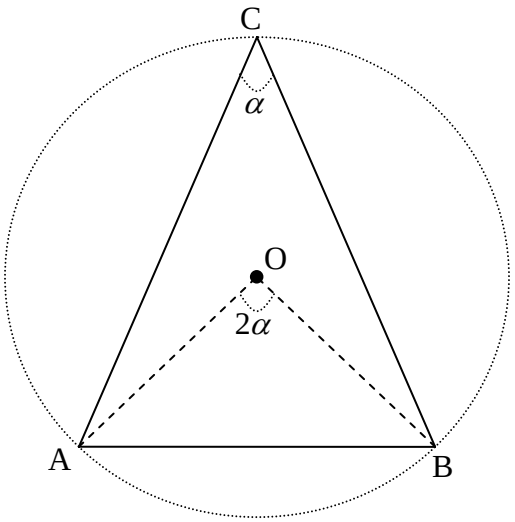

O is inside $\Delta ABC \Rightarrow \quad 2\alpha < 180$

$\Rightarrow \quad \alpha < 90$

O is outside $\Delta ABC \Rightarrow \quad 2\alpha > 180$

$\Rightarrow \quad \alpha > 90$

Figure 10: The upper bound on *M* (ratio of circumradius to smallest triangular edge) is controlled inversely by an angle α that is subtended by the smallest side AB of the triangular element on the opposite vertex.

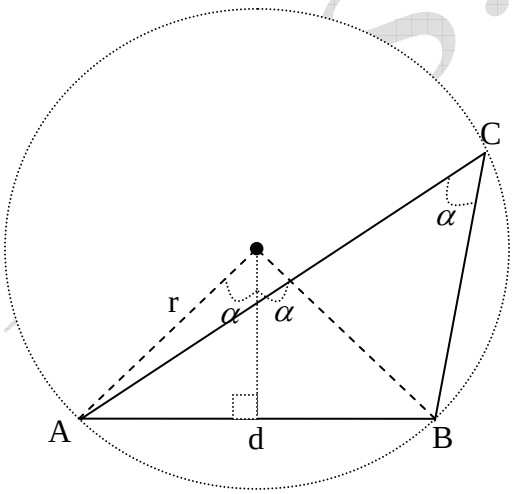

$$M = \frac{r}{d} \qquad Sin\alpha = \frac{d/2}{r}$$

$$\Rightarrow Sin\alpha = \frac{1}{2M} \qquad \Rightarrow \alpha = Sin^{-1}(\frac{1}{2M})$$

Figure 11: Top left unstructured mesh decomposition (UnSrG) is generated based on thematic class (soil type) boundary as constraint. Top right structured mesh (SrG) decomposition has same spatial resolution as the grid on left. Colored grid in the background of both the decompositions is a soil type map. The zoomed-in image shows that SrG (in light grey) have multiple soil classes within them. UnSrG edges (in red or dark grey (in black and white)) overlap soil class edges thus resulting in a "one soil class assignment" to each triangle

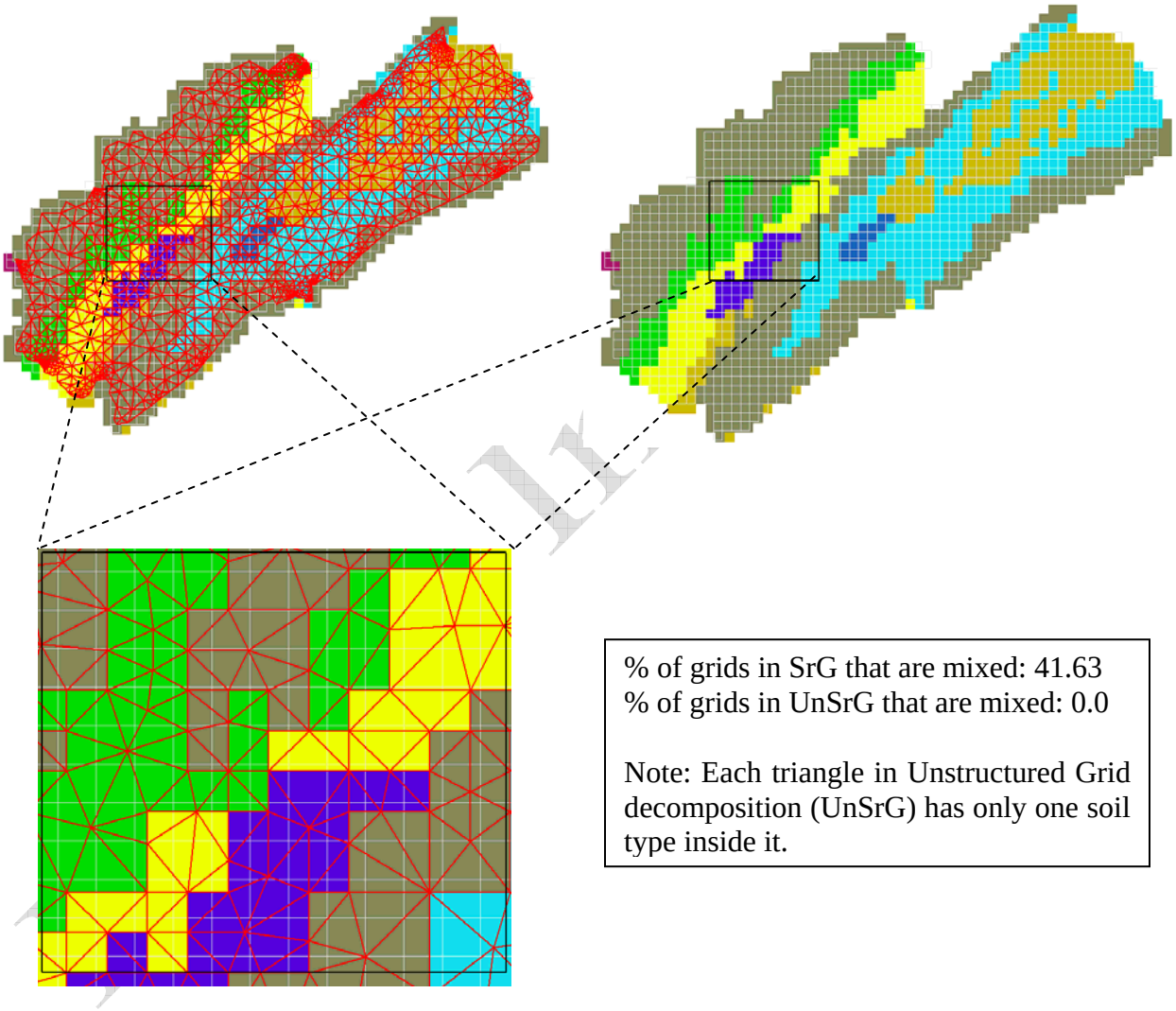

% of grids in SrG that are mixed: 41.63
% of grids in UnSrG that are mixed: 0.0

Note: Each triangle in Unstructured Grid decomposition (UnSrG) has only one soil type inside it.

Figure 12: Left figure shows the elevation hypsometric curve of Little Juniata Watershed. Delaunay Triangulation of Little Juniata Watershed while using hypsometric division as a constraint. Expectedly in regions of higher topographic extremes/gradient, concentration of meshes is higher. Note the formation of smaller triangles besides the streams. Similar divisional constraints can be used for vegetation and climate regimes.

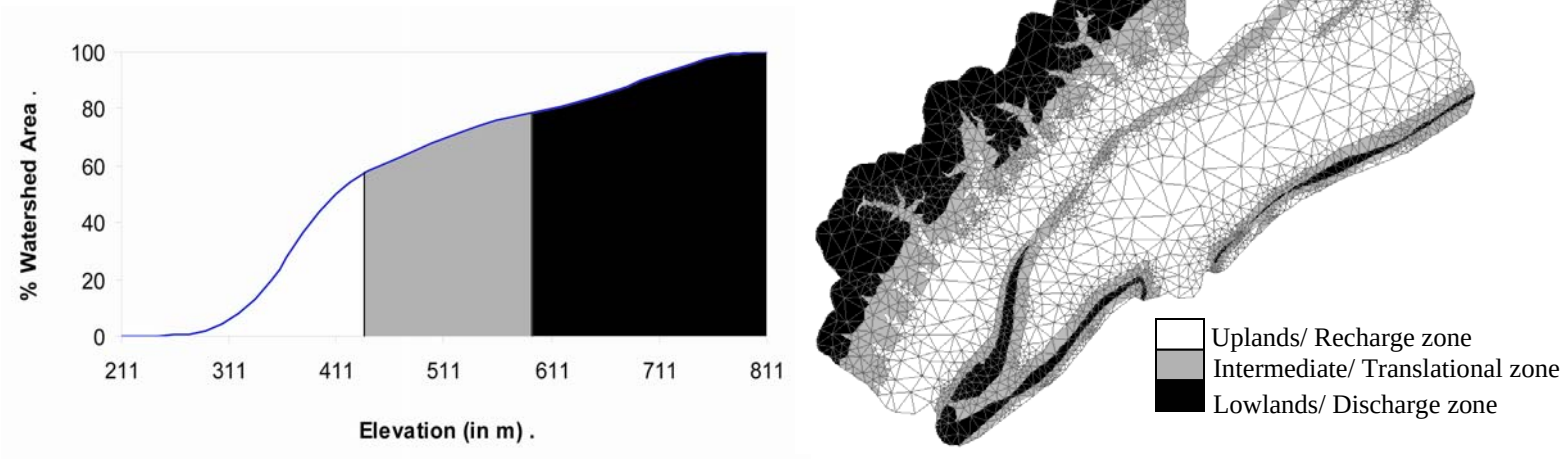

Figure 13: Domain decomposition of Great Salt Lake Basin. Note that no triangles are created inside the lake.

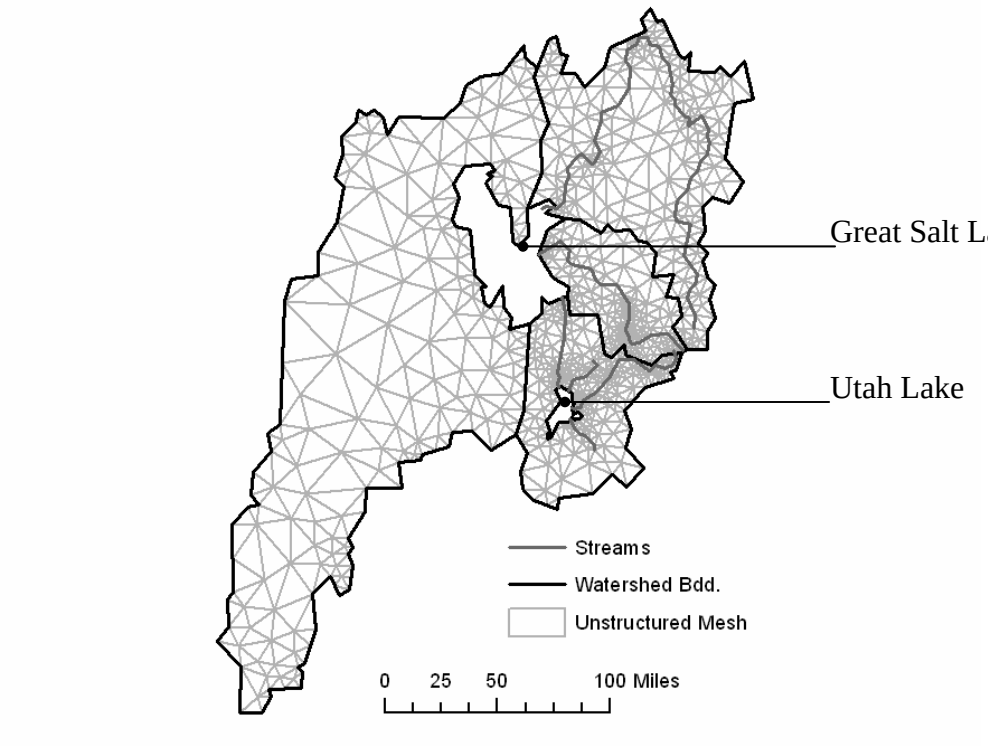

Figure 14: (a) Zoom-in of mesh decomposition with and without using groundwater observation stations as constraints for two locations inside the watershed (b) Mesh decomposition with (right side, green) and without (left side, grey) using observation stations as constraints (c) Zoom-in of mesh decomposition with and without using stage observation stations as constraints for two locations on Little Juniata River. We note that in constrained decomposition, triangulations are generated such that the observation stations lie directly on the mesh nodes.

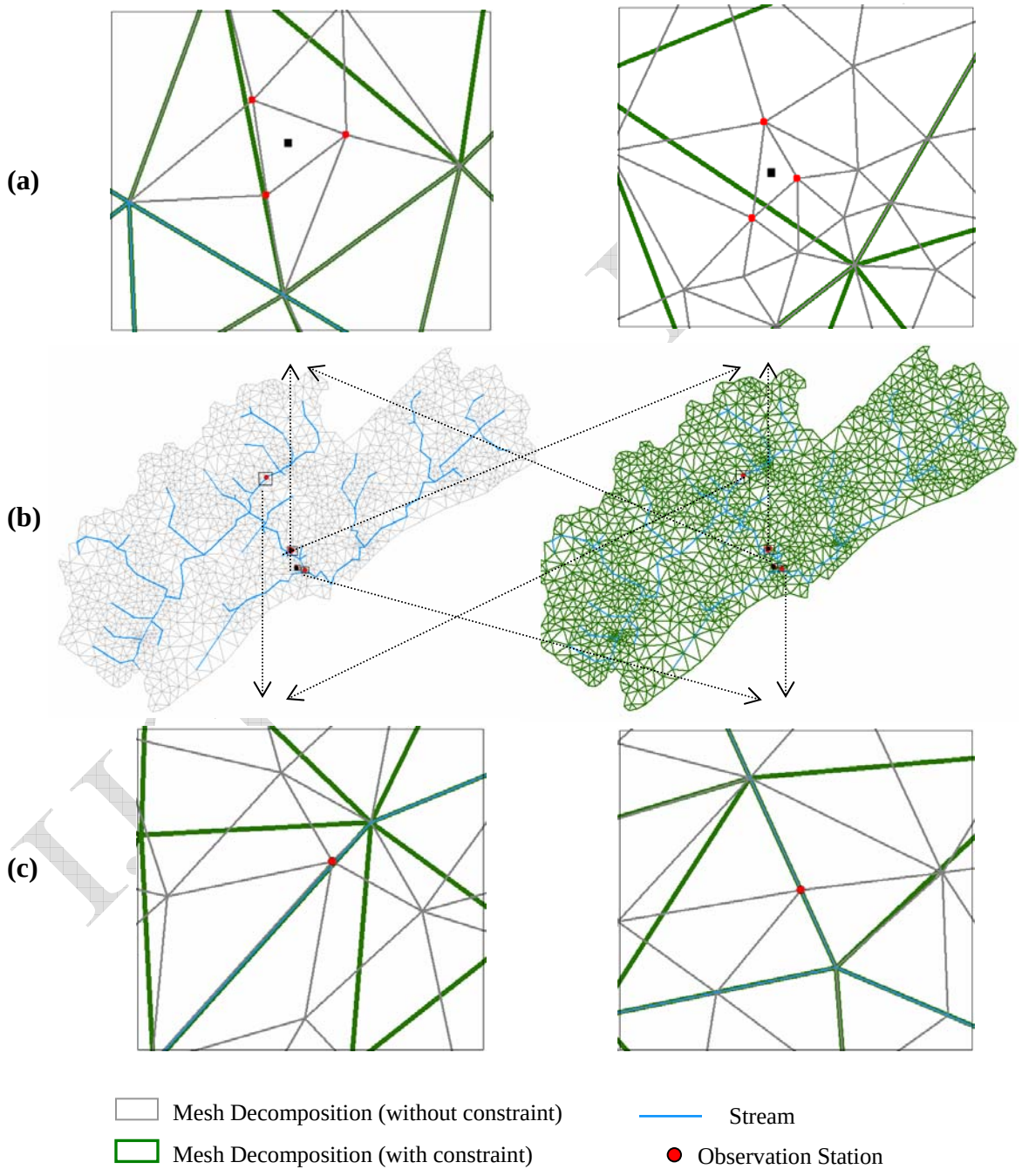

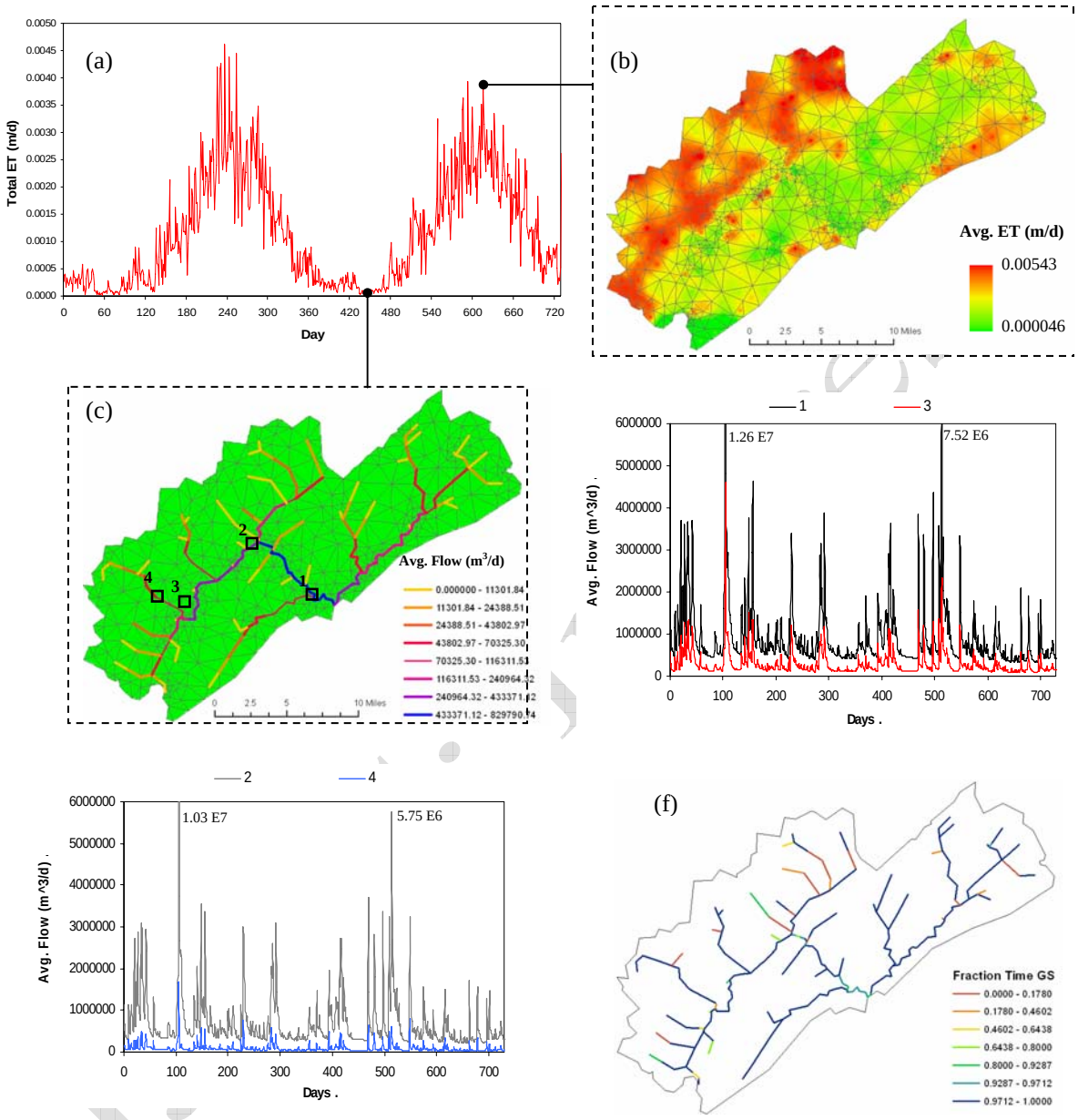

Figure 15: (a) shows the average evapo-transpiration (ET) time series for the Little Juniata watershed for two year period. Snapshots for spatial distribution of ET during the maximum and minimum extremes are shown in (b) and (c) respectively. Since we have used same color range to represent both extremes, ET appears to be uniform everywhere (though that is not the case) during winter as the values are quite small. (d) and (e) shows the streamflow hydrograph at four locations in the stream network. (f) shows the percentage of time each stream segment gains water from the aquifer. We note that all the results shown above are for a simulation period of 2 years ranging from Nov, 1983 to Oct. 1985.

Figure 16: Nested Mesh decomposition of Little Juniata Watershed while using subsheds as internal boundary. For computational efficiency a localized region of the basin (around main stem of Little Juniata River, shaded in the figure) can be discretized to higher spatial resolution elements while leaving rest of the basin at coarser resolution. Under a single framework, mesoscale to microscale modeling can be performed.

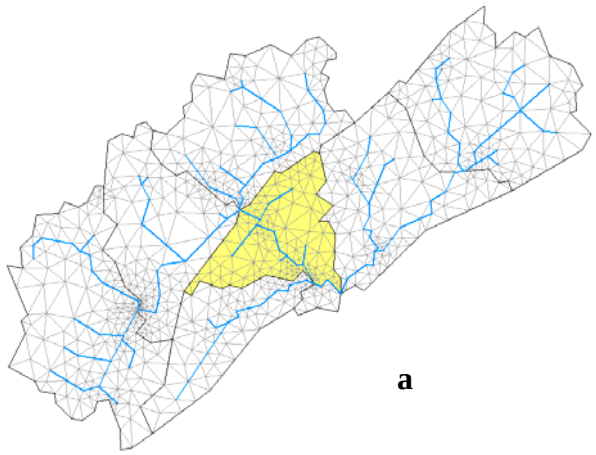

a

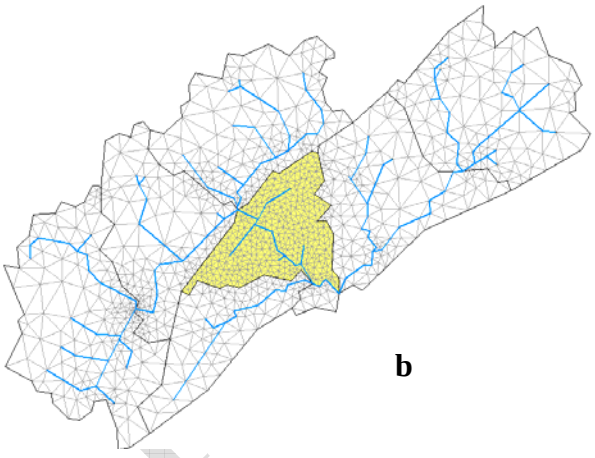

b

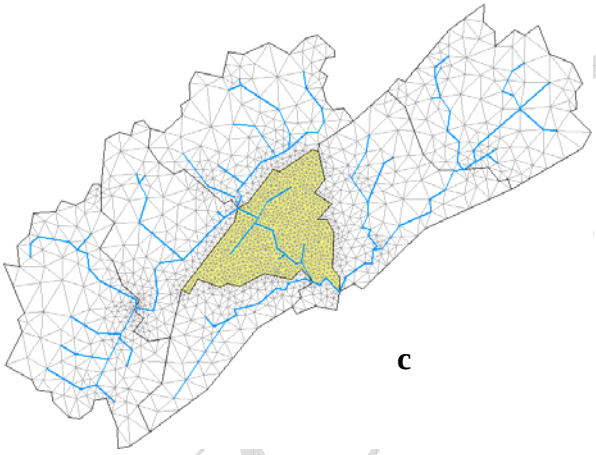

c

Maximum area of triangle in targeted nested zone in **(a)** : 2 sq. km

Maximum area of triangle in targeted nested zone in **(b)** : 0.2 sq km

Maximum area of triangle in targeted nested zone in **(c)** : 0.01 sq km

Figure 17: Flow chart depicting the dynamically adaptive refinement/de-refinement algorithm for hydrologic modeling. Depending on the hydrodynamics, a particular region can be refined to finer or coarse triangular elements in order to capture the hydrologic process accurately.

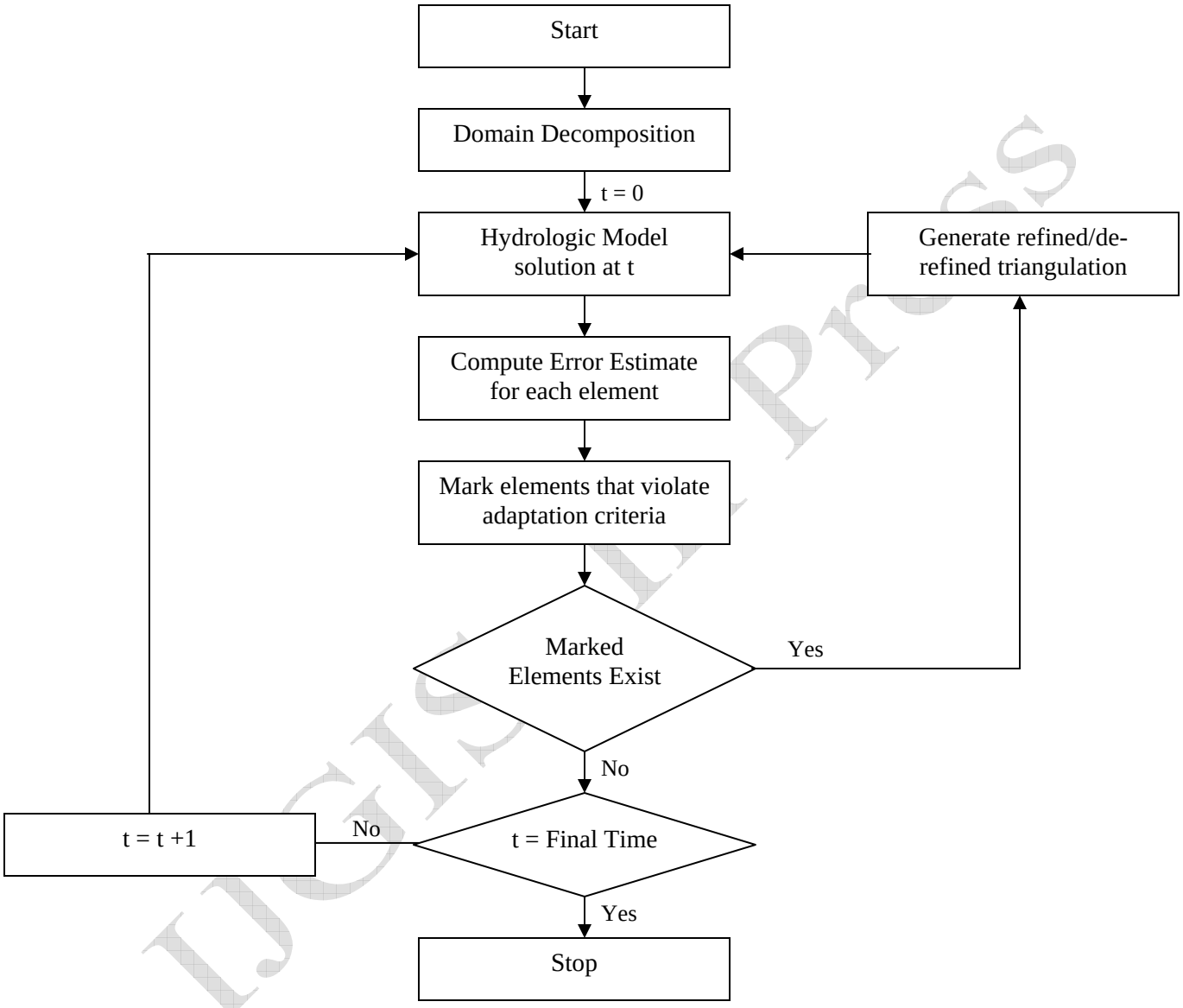

Figure 18: Coarse-scale unstructured mesh decomposition of Little Juniata Watershed (Left). At any time *t* during simulation, two triangles (cyan) are marked as Bad Elements depending on spatial gradient estimate of a state variable and are identified for refinement. Decomposition on the right shows insertion of a node inside the marked elements and the resulting perturbed region. Note the formation of new triangles and the triangulated area that gets perturbed is very small relative to the whole watershed. Triangles in the unperturbed region remain same.